Local and Regional Enhancements of CH_4, CO, and CO_2 Inferred from TCCON Column Measurements

Kavitha Mottungan[1,a], Chayan Roychoudhury[1], Vanessa Brocchi[1,b], Benjamin Gaubert[3], Wenfu Tang[3], Mohammad Amin Mirrezaei[1], John McKinnon[1], Yafang Guo[1], David W.T. Griffith[4], Dietrich Feist[5], Isamu Morino[6], Mahesh K. Sha[7], Manvendra K. Dubey[8], Martine De Mazière[7], Nicholas M. Deutscher[4], Paul O. Wennberg[9], Ralf Sussmann[10], Rigel Kivi[11], Tae-Young Goo[12], Voltaire A. Velazco[13], Wei Wang[14], Avelino F. Arellano Jr.[1,2]

[1] Department of Hydrology and Atmospheric Sciences, University of Arizona, Tucson, 85721, USA
[2] Department of Chemical and Environmental Engineering, University of Arizona, Tucson, 85721, USA
[3] NSF National Center for Atmospheric Research, Boulder, CO, 80307, USA
[4]Centre for Atmospheric Chemistry, School of Earth, Atmospheric and Life Sciences, University of Wollongong, Wollongong, Australia
[5]Institut für Physik der Atmosphäre, Deutsches Zentrum für Luft- und Raumfahrt (DLR), Oberpfaffenhofen, Germany
[6]National Institute for Environmental Studies (NIES), Onogawa 16-2, Tsukuba, Ibaraki 305-8506, Japan
[7]Royal Belgian Institute for Space Aeronomy (BIRA-IASB), Brussels, Belgium
[8]Los Alamos National Laboratory, Earth Systems Observations (EES-14), United States
[9]Division of Engineering and Applied Science, California Institute of Technology, Pasadena, CA, USA
[10]Karlsruhe Institute of Technology, IMK-IFU, Germany
[11]Space and Earth Observation Centre, Finnish Meteorological Institute, Sodankylä, Finland
[12]Convergence Meteorological Research Department, National Institute of Meteorological Sciences (NIMS), Seogwipo-si 63568, Korea
[13]Deutscher Wetterdienst (DWD), Meteorological Observatory Hohenpeissenberg, 82383 Hohenpeissenberg Germany
[14]Key Laboratory of Environmental Optics and Technology, Anhui Institute of Optics and Fine Mechanics, Hefei, China

[a] now at: National Physical Laboratory (NPL), Teddington, UK
[b] now at: Atmo Auvergne-Rhône-Alpes, association agréé de surveillance de la qualité de l'air, 69500 Bron, France

Correspondence to: Avelino Arellano (afarellano@arizona.edu)

Abstract. In this study, we demonstrate the utility of available correlative measurements of carbon species to identify regional and local airmass characteristics and their associated source types. In particular, we combine different regression techniques and enhancement ratio algorithms with carbon monoxide (CO), carbon dioxide (CO_2), and methane (CH_4) total column abundance from 11 sites of the Total Carbon Column Observing Network (TCCON) to infer relative contributions of regional and local sources to each of these sites. The enhancement ratios provide a viable alternative to univariate measures of relationships between the trace gases that are insufficient in capturing source type and transport signatures. Regional enhancements are estimated from the difference between bivariate regressions across a specific time window of observed total abundance of these species (BERr) and inferred anomalies (AERr) associated with a site-specific background. Since BERr and

AERr represent the bulk and local species enhancement ratio, respectively, its difference simply represents the site-specific regional component of these ratios. We can then compare these enhancements for CO_2 and CH_4 with CO to differentiate combustion versus non-combustion associated airmasses. Our results show that while the regional and local influences in enhancements vary across sites, dominant characteristics are found to be consistent with previous studies over these sites and with bottom-up anthropogenic and fire emission inventories. The site in Pasadena shows a dominant local influence (>60%) across all species enhancement ratios, which appear to come from a mixture of biospheric and combustion activities. In contrast, Anmyeondo shows more regionally influenced (>60%) air masses associated with high temperature and/or biofuel combustion activities. Ascension appears to only show a large regional influence (>80%) on CO/CO_2 and CO/CH_4 which is indicative of transported and combustion-related CO from nearby African region, consistent with sharp rise in column CO (3.51±0.43 % ppb/year) in this site. These methods have important application to source analysis using space-borne column retrievals of these species.

1 Introduction

The rise in the abundance of greenhouse gases (e.g., CO_2 (carbon dioxide), CH_4 (methane)) in recent decades, because of anthropogenic activities and natural emissions associated with climate change, such as wetland, and biomass burning emissions associated with El-Niño (Zhang et al., 2018; Kumar et al., 2023; van Vuuren and Riahi, 2008; Arneth et al., 2017), has large implications to quantifying atmospheric chemistry-climate relationships. This rising trend increases the complexity in understanding the feedback mechanism (CH_4-OH (hydroxyl)-CO (carbon monoxide)), retrieval bias in less validated regions or unresolved uncertainty in tropical emissions (e.g., based on TROPOspheric Monitoring Instrument (TROPOMI) and Greenhouse Gases Observing Satellite **(**GOSAT)) (Lunt et al., 2019; Palmer et al., 2019) and emission estimates from fossil-fuel use over growing megacities (Tang et al., 2020; Maasakkers et al., 2019). Understanding today's regional CO_2 and CH_4 sources and sinks is a key area in carbon cycle and atmospheric composition science given the necessity for reliable projections of future atmospheric CO_2 and CH_4 concentrations. This is especially problematic in megacities with the fastest pace of urbanization and where the anthropogenic activities are most intense, accompanied by immense energy consumption mainly in the form of fossil-fuel combustion (Kennedy et al., 2015; Grimm et al., 2008; Agudelo-Vera et al., 2012; Banerjee et al., 1999; Lamb et al., 2021). Emission estimates from fossil-fuels remain uncertain due to poor characterization of combustion activity, efficiency and fuel-use mixtures emerging from the lack of details on pollution control strategies, energy use and combustion practices (Zhu et al., 2012; Creutzig et al., 2015; Kennedy et al., 2009; Baiocchi et al. 2015; Weisz and Steinberger, 2010; Bettencourt et al., 2007; Dodman, 2009, Bai et al., 2018). The high-efficiency combustion of fossil-fuels leads to large CO_2 emissions compared to CO, whereas low-efficiency combustion of residential combustion, biomass burning, among others produce more CO (Andreae and Merlet 2001; Silva and Arellano, 2017; Halliday et al., 2019; Tang et al., 2019; Wei et al., 2012; Andreae, 2019; Park et al., 2021). This uncertainty is further complicated by limited observations at the spatiotemporal scales necessary to resolve variations in combustion and fuel-use patterns (Streets et al., 2013; Nassar et al., 2013; Hutyra et al., 2014, Gately and Hutyra 2017; Creutzig et al., 2019; Arioli et al., 2020). This leads to difficulties in teasing out small anthropogenic signatures from the large natural sources and sinks dominating the carbon cycle and the uncertainties in modelling atmospheric transport (Peylin et al., 2013; Thompson et al., 2016; Erickson and Morgenstern, 2016; Oda et al., 2019; Duncan et al., 2019; Gaubert et al., 2019). This is especially true for flux

estimations of CO_2 and CH_4 using top-down approaches, despite the increase in aircraft and satellite measurements of CO_2 and CH_4 abundance in recent years (Hutyra et al., 2014; Houweling et al., 2015; 2017, Chevallier et al., 2019; Crowell et al., 2019; Lu et al., 2021; Chandra et al., 2021). Studies have also highlighted the importance of fossil-fuel emission uncertainties on their estimates, suggesting the need for temporally defined emission inventories (Gurney et al., 2005; Peylin et al., 2011; Thompson et al., 2016, Saeki and Patra, 2017; Gurney et al., 2020).

The abundance of a species at a particular location is mainly dependent on the variations of sources and sink. Furthermore, both regional and local transport (long-range, vertical transport and dilution in the boundary layer) influence the abundance of the species (especially in the column) and confound measurement interpretations. The major sources of CO_2 include anthropogenic emissions especially fossil-fuel combustion, cement production, and land-use change while sinks include uptakes by ocean and land from the atmosphere (Friedlingstein et al., 2022). While CO is primarily produced through incomplete combustion of carbon-containing fuels, oxidation of CH_4 and other volatile organic compounds by OH contributes to the secondary production of CO (Bakwin et al., 1995; Gaubert et al., 2016, Hoesly et al., 2018). The main chemical sink of CO in the atmosphere is OH followed by dry deposition through soil uptake (Levy 1971, Bartholomew 1981, Khalil and Rasmussen, 1990, Cordero et al., 2019). This coupling of CH_4-OH-CO has significant impact on the growth rate and source-sink characterization of CH_4 (Gaubert et al., 2017; Zhao et al., 2019; 2020; Guthrie, 1989; Prather, 1994; Lelieveld et al., 2002). Anthropogenic sources of CH_4 include agricultural activities (rice and livestock), solid waste, fossil-fuels, and biomass burning in addition to natural sources like anaerobic ecosystems and geological activities (Saunois et al., 2020; Stavert et al., 2022). CH_4 and CO are thus coupled with common sources (combustion process, vehicular emission, etc.) and sink (OH) and changes in one of these species will have a significant impact on the other (Sze, 1977; Gaubert et al., 2017). This co-variation (co-emission) or the correlations of the species can be used to derive enhancement ratios/emission ratios which vary according to source regions and source type (Palmer et al., 2006; Wang et al., 2010; Tang et al., 2018). For example, a recent study by Lelandais et al. (2023) uses enhancement ratios and correlations to study variability of ICOS (Integrated Carbon Observation System)-France observed CO, CO_2, and CH_4 in a Mediterranean climate at different regional and time scales. Their results showed 84% of their data was representative of background concentrations that were dependent on both wind speed and direction, while 16% were enhanced by anthropogenic plumes, emissions in the boundary layer, or short-term pollution events. Emission (enhancement) ratios are defined as ratios of excess abundance across two species, often in units of mass flux (molar) when the concentrations of the species are estimated near (away from) the emission source (Andreae, 2019; Lefer et al., 1994). These derived emission or enhancement ratios from multiple species are widely used to characterize emission sources and flux estimation for different parts of the world (Turnbull et al., 2011, 2015; Silva et al., 2013; Anderson et al., 2014; Ammoura et al., 2014; Popa et al., 2014; Parker et al., 2016; Silva and Arellano, 2017; Bukosa et al., 2019; Tang et al., 2019; Lee et al., 2020; Sim et al., 2022; Djuricin et al., 2010) (Wunch et al., 2009; Miller et al., 2012; Wennberg et al., 2012; Bozhinova et al., 2014; Super et al., 2017; Hedelius et al., 2018, Plant et al., 2022; Bares et al., 2018). For example, a recent study by Plant et al. (2022) investigated the urban emissions of CH_4 and CO using enhancement ratios derived from TROPOMI while Halliday et al. (2019) characterized air masses

during KORUS-AQ into regions of high or low-efficiency combustion based on CO/CO_2 enhancement ratios derived from aircraft data. Bukosa et al. 2019 used shipborne measurements of CO, CO_2, and CH_4 to improve GHG flux estimates by comparing them with GEOS-Chem simulations to identify missing/underestimated sources in the model.

The enhancement ratio between species *X* and *Y* is calculated by mainly two methods: the first is from a linearly regressed slope of *X* and *Y* (Andreae et al., 1988a, 1988b) and the second is by dividing the excess of *X* by the excess of *Y* (Andreae and Merlet, 2001) (See Methods 1 and 2 in Sect. 2.2 respectively). The first approach of enhancement ratio estimation using regression slopes is difficult to infer when emitted or locally produced species mix with different air masses (e.g., advection from the nearby sources or mixed air masses) downwind of the dominant source where measurements are made. This is especially the case for vertically integrated quantities like the column measurements (either ground-, aircraft- and satellite-based) (Cheng et al., 2017; Halliday et al., 2019; Tang et al., 2019) where vertical information of the species abundance is practically absent. If the emission or plume concentration is significantly larger than the background, the ratio from the regression slope approach does not change (Brigg et al., 2016). But, when emission of the species mixes with different 'backgrounds' than a relatively uniform field, the abundances of *X* and *Y* change due to mixing and/or photochemical loss (Mauzerall et al., 1998; Yokelson et al., 2013; Guyon et al., 2005); thus, making it difficult to track the locally emitted contribution to the observed abundance. The latter approach of using excess of the species requires a proper understanding of the background concentration to derive the excess abundance along with the instantaneous concentration of the species, which is not available in most cases. Vertical and horizontal transport also complicates the interpretation of abundance and assessment of local and regional source influences at a particular location (Chatfield et al., 2020). A combination of these two approaches have also been used in previous studies (Hedelius et al., 2018) (Method 3 in Sect. 2.2). Here, we utilize the column measurements of CO, CO_2, and CH_4 (denoted as X_{CO}, X_{CO2}, X_{CH4}) from the Total Carbon Column Observing Network (TCCON) (Wunch et al., 2011) to understand these variations in the column abundances.

The main objective of this study is to characterize the bulk characteristics of X_{CO}, X_{CO2}, and X_{CH4} from ground-based TCCON measurements using a combination of enhancement ratio approaches. Specifically, we introduce a combination of established local and bulk regression algorithms in deriving enhancement ratios of the column abundances between these three species to understand their relationships because these constituents are being mixed, dispersed, transported, and transformed in the atmosphere. More importantly, we present the utility of combining these techniques in quantifying the contributions of the regional and local influences to observed columns and the corresponding enhancements observed in the respective species. We then examine the regional and seasonal variations of these influences and make use of the variability in the relationship of the multi-species enhancement ratios to infer the dominant source type leading to these variations. While previous studies have used enhancement ratios to examine the source attribution of X_{CO}, X_{CO2}, and X_{CH4} at a regional and/or local scale (Bukosa et al., 2019), the novelty of this study lies in investigating the bulk characteristics on a source type basis using all three species and using a combination of different regression algorithms for globally distributed column-integrated measurements. This proof-of-concept has an important

application to on-going and planned satellite missions of these species given that TCCON measurements serve as basis for retrieval validation of these missions.

2 Data and Methods

2.1 Data and Location Features

We make use of the column-averaged mixing ratios of CO, CO_2, and CH_4 (denoted as X_{CO}, X_{CO2}, X_{CH4}) from the ground-based network of TCCON during 2012 to 2019. TCCON retrieves the column abundance from the near-infrared solar absorption spectra using high-resolution Fourier transform spectrometers (Wunch et al., 2011). This network provides the column-averaged dry-air mole fractions by normalizing the column abundance of the species of interest to the retrieved oxygen column abundance. The precision of the column-averaged mole fraction of CO_2 (X_{CO2}) is <0.25 %, CH_4 (X_{CH4}) is <0.3% and CO (X_{CO}) is <1% under clear or partly cloudy skies (Wunch et al., 2010). TCCON datasets are widely used in global carbon cycle studies to improve the carbon budget (source and sinks information) and for validation of atmospheric trace gas estimates retrieved from the space-based instruments such as Orbiting Carbon Observatory (OCO-2), GOSAT, GOSAT-2, and TROPOMI, (Miller et al., 2007; Morino et al., 2011; Frankenberg et al., 2015; Wunch et al., 2017; Qu et al., 2021; Wang et al., 2022; Kulawik et al., 2016; Yoshida et al., 2013; Noël et al., 2022; Liang et al. 2017; Kong et al., 2019; Sha et al., 2021). A total of 11 TCCON sites are selected for this analysis which includes six sites in the Northern Hemispheric (NH) regions and five in the Southern Hemispheric (SH) regions and the locations are marked in Figure 1. The average column abundance retrieved at each TCCON location is embedded in the monthly averaged spatial map of X_{CO} from the Measurements of Pollution In The Troposphere (MOPITT) aboard Terra, X_{CO2} from OCO-2 and GOSAT retrieved X_{CH4} during 2012 - 2019. X_{CO} and X_{CH4} from MOPITT (and GOSAT) show good agreement with Pearson's correlation of 0.96 (and 0.97) and mean bias relative to TCCON of -12.81 ppb (-7.12 ppb). OCO-2 X_{CO2}, on the other hand, has a higher bias and weaker correlation relative to TCCON (correlation of 0.6 and bias of 1.95 ppm) with the least (highest) bias in Pasadena (Manaus). The monthly mean variations in the three species across the sites shown in Figure S3 highlight the hemispheric differences of X_{CO}, X_{CO2}, and X_{CH4} among TCCON locations.

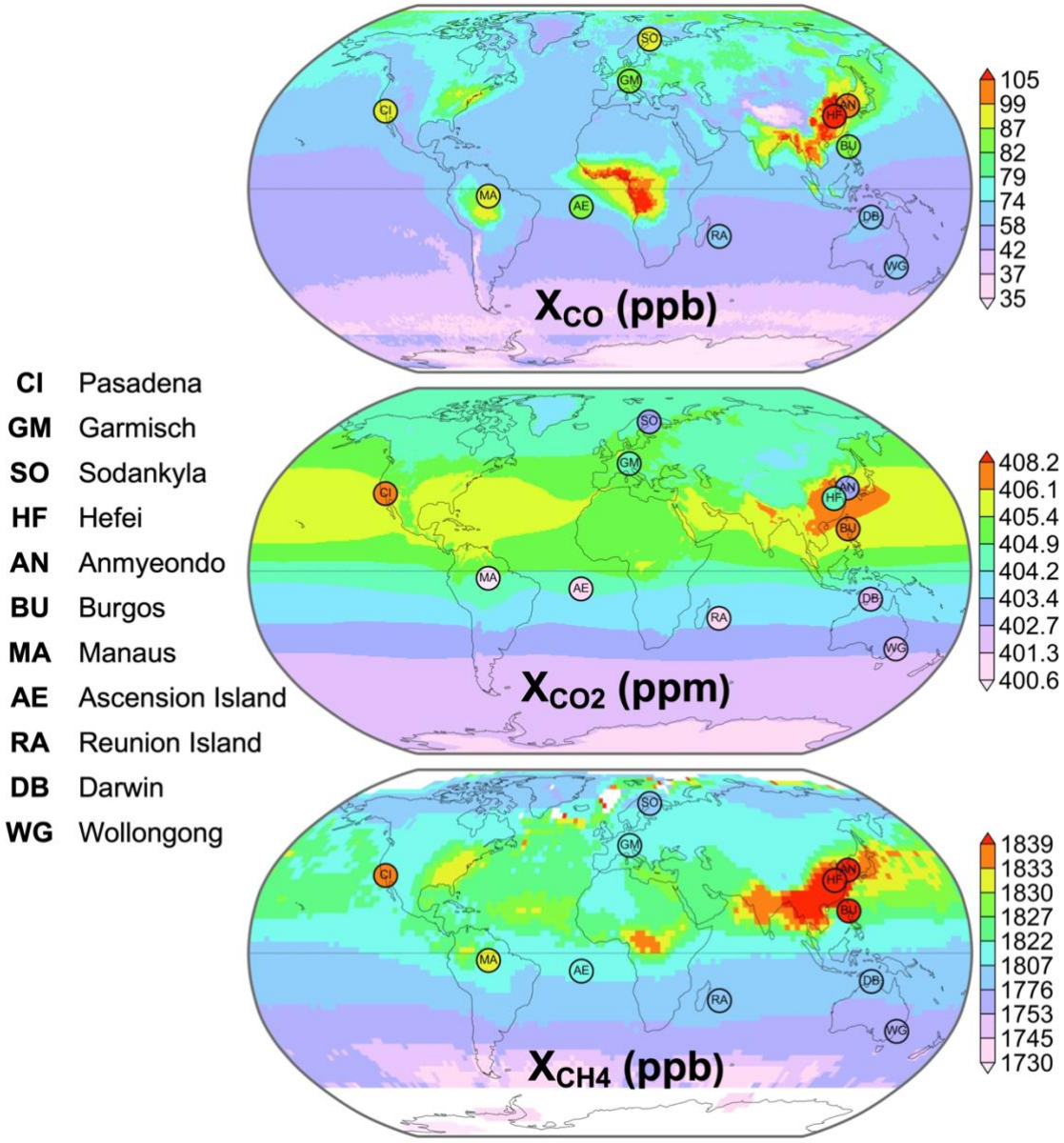

Figure 1: Month-average abundance of: (a) CO from MOPITT between 2012 - 2019, (b) CO_2 from OCO-2 between 2015 - 2019, and (c) CH_4 from GOSAT-1 between 2012 - 2019. Locations of TCCON sites are superimposed as black circles with their respective TCCON ID (left legend).

195 The site in Ascension is in a small island with virtually no influence from local sources, but it captures the long-range transport of emissions from Africa (Geibel et al., 2010; Feist et al., 2014, Swap et al., 1996). A significant positive trend in X_{CO} is observed in Ascension (3.51±0.43 % ppb/year) with negative X_{CO} trends in the other sites (Table 2). This can be attributed to increase in burned area and transport from southern Africa reported in previous studies (Buchholz et al., 2021; Andela et al., 2017,
200 Borsdorff et al., 2018). This in combination with the low trend observed in X_{CO2} over Ascension may be

attributed to a decrease in sources (reduced respiration, increase in lower quality fossil-fuels) or an increase in sinks (enhanced photosynthesis) over the African region. Hickman et al., 2021 reported an increasing trend in CO over north equatorial Africa due to decline in biomass burning emissions from a woodier biome. Among the selected sites of study, Ascension and Reunion are representative of remote island sites located in the South Atlantic and the Indian Ocean, respectively. The humidity in the eastern part of the Reunion Island is higher than its western counterpart. There is also a regularly occurring outflow of biomass burning emission from South Africa, Madagascar, and South America to Reunion Island (Vigouroux et al., 2012; De Maziere et al., 2017; Zhou et al., 2018). The sites in Manaus, Darwin, Garmisch, and Sodankylä are reported to be mostly influenced by sources related to local biogenic emissions and regional anthropogenic emissions. Manaus is in the center of the Amazon, the world's largest rainforest, and is the seventh largest city in Brazil (Dubey et al., 2014). The measurement site in Garmisch is situated in the Alps Mountain range in Southern Germany (Sussmann and Rettinger, 2018) while the site in Sodankylä in Northern Finland, mainly surrounded by Scots pine forest within the Fennoscandia region. Wintertime measurements at this location is not possible due to the absence of sunlight (Kivi et al., 2014). Finally, Darwin is the largest city in the sparsely populated Northern Territory of Australia and is situated on the Timor Sea. The site is 9 km from the city of Darwin and adjacent to the airport (Griffith et al., 2014).

It has been previously reported that local emissions and nearby sources are significant at Pasadena, Anmyeondo, and Wollongong (Griffith et al., 2014; Wennberg et al., 2015; Goo et al., 2014). The measurement site in Pasadena is situated at the northern limit of the South Coast air basin, which is bounded by mountains on three sides and the Pacific Ocean on the other side. The northern and eastern regions of the basin are sparsely populated deserts and receives polluted air under normal meteorological conditions and occasionally cleaner air (Wunch et al., 2009; Wennberg et al., 2012). In SH, the measurement site of Wollongong is representative of an urban location. The urban sources are local and is mainly from Sydney's motorway flanks, coal mining, steelmaking facilities (Buccholz et al., 2016). Biogenic emission and bush fire also impact the air at this site along with agricultural activities in the southwest side of the urban extent (Griffith et al., 2014; Buchholz et al., 2016). Anmyeondo Island is located on the west coast of the Korean Peninsula, 180 km southeast of Seoul. Although surrounding area mainly consists of agricultural lands, vegetation in and around the sites consisting of pine trees, natural forest, and urban developments, this site is regularly influenced by Asian pollution outflows especially during Spring (Goo et al., 2014; Oh et al., 2018). From Table 2, Increased X_{CO2} and X_{CH4} trends are observed at all locations. The trend in X_{CO2} is highest over Anmyeondo (0.81± 0.10 % ppm/year), and lowest over Ascension, (0.60±0.01 % ppm/year). Similarly, X_{CH4} shows a high trend in Sodankylä (0.48±0.02 % ppm/year) a low trend in Anmyeondo (0.21± 0.15 % ppm/year). This is possibly due to differences in the distribution of sources and/or sinks across these sites as described in the previous paragraphs.

The air in Burgos and Hefei sites are mainly dominated by regionally transported emissions (Morino et al., 2018; Liu et al., 2018). The average X_{CO} is high in these regions (also Anmyeondo) compared to other sites (Table 2) which is consistent with previous literature that reports higher emissions from fossil-fuels, coal, agricultural activities and wetlands (Tang et al., 2019; Zhang et al., 2020). Hefei is an inland city in the eastern part of China, and it is a rapidly developing city with a population of eight

million. The site is adjacent to a lake in flat terrain and is in the north-western rural area of Hefei city. A large anthropogenic influence in Hefei comes mainly from heavily polluted areas in northern China and cities in the Yangtze River Delta, while natural emissions come from cultivated lands or wetlands surrounding the site (Tian et al., 2018; Wang et al., 2017). The site in Burgos is in a town in Ilocos Norte Province in the Philippines. This region is a coal-free province and encounters relatively clean marine air from the western Pacific but also polluted air from long-range transport during monsoon transitions (Velazco et al., 2017). The data period and a summary of the characteristics of these selected TCCON sites are listed in Table 1. The sites at Pasadena, Garmisch, Reunion, Ascension, Sodankylä, Darwin, and Wollongong have longer records (> 7 years of data) as opposed to Anmyeondo, Hefei, Manaus, and Burgos (~2 years with more gaps in between).

Table 1: Relevant reference and acknowledgement on selected TCCON sites considered in this work.

Location	Data Period	Longitude	Latitude	Site Reference	Data Reference	DOI	Source Features
Pasadena	09/2012-08/2019	-118.13	34.14	Wennberg et al., 2015		10.14291/tccon.ggg2014.pasadena01.R1/1182415	Local and Regional
Ascension	05/2012-10/2018	-14.33	-7.92	Geibel et al., 2010	Feist et al., 2014	10.14291/tccon.ggg2014.ascension01.R0/1149285	Remote
Manaus	10/2014-06/2015	-60.60	-3.21		Dubey et al., 2014	10.14291/tccon.ggg2014.manaus01.R0/1149274	Local and Regional
Garmisch	07/2007-08/2019	11.06	47.48		Sussmann and Rettinger, 2018;	10.14291/tccon.ggg2014.garmisch01.R2	Local and Regional
Sodankylä	05/2009-06/2019	26.63	67.37		Kivi et al., 2014	10.14291/tccon.ggg2014.sodankyla01.R0/1149280	Local and Regional
Anmyeondo	02/2015-04/2018	126.33	36.54		Goo et al., 2014	10.14291/tccon.ggg2014.anmeyondo01.R0/1149284	Local and Regional
Burgos	03/2017-11/2018	120.65	18.53	Morino et al., 2018	Velazco et al., 2017	10.14291/tccon.ggg2014.burgos01.R0/1368175	Regional
Hefei	09/2015-12/2016	117.17	31.90	Liu et al., 2018	Wang et al., 2017	10.14291/tccon.ggg2014.hefei01.R0	Regional
Darwin		130.90	-12.44				

	08/2005-09/2018			Griffith et al., 2014	Deutscher et al., 2010	10.14291/tccon.ggg2014.darwin01.R0/1149290	Local and Regional
Wollongong	06/2008-11/2018	150.88	-34.41	Griffith et al., 2014		10.14291/tccon.ggg2014.wollongong01.R0/1149291	Local and Regional
Reunion	09/2011-02/2018	55.49	-20.90		De Maziere et al., 2017	10.14291/tccon.ggg2014.reunion01.R1	Local and Regional

2.2 Estimating regional and local enhancement ratios

The observed column abundance (C) of any species (spc) retrieved at any location of TCCON measurement site (s) and at a particular time (t) is generally represented as:

$$C_{spc} = C_{true,spc} + \epsilon_{meas,spc} \quad (1)$$

where C_{true} is the true species concentration being measured at (s,t) and ϵ_{meas} is the measurement error. Letting $C_X = C_{CO_2}$, $C_Y = C_{CO}$, and $C_Z = C_{CH_4}$, the true concentration can be broken down into specific contributions following Levin et al., 2003 and Turnbull et al., 2009 as:

$$C_X = (\mathrm{X}_{bg} + \mathrm{X}_{ff} + \mathrm{X}_{bb} + \mathrm{X}_c + \mathrm{X}_r - \mathrm{X}_p) + \epsilon_X \quad (2)$$

$$C_Y = (\mathrm{Y}_{bg} + \mathrm{Y}_{ff} + \mathrm{Y}_{bb} + \mathrm{Y}_{ox} - \mathrm{Y}_l - \mathrm{Y}_{su}) + \epsilon_Y \quad (3)$$

$$C_Z = (\mathrm{Z}_{bg} + \mathrm{Z}_{ff} + \mathrm{Z}_{bb} + \mathrm{Z}_{wet} + \mathrm{Z}_{live} + \mathrm{Z}_{oth} - \mathrm{Z}_{cl} - \mathrm{Z}_{su}) + \epsilon_Z \quad (4)$$

The subscripts in the above equations represent the associated sources and sinks: background (bg); anthropogenic processes such as fossil-fuel (ff), biomass burning (bb), cement (c), and livestock ($live$); biospheric processes such as ecosystem respiration (r) and photosynthesis uptake (p); natural processes such as ocean (o), soil uptake (su), and wetland (wet); chemical processes such as oxidation from hydrocarbons (ox), chemical loss by OH (l), chemical loss by OH and Cl (cl); and other sources (oth). The background component (bg) accounts for initial abundance, dilution, and transport processes. Direct biogenic CO emissions and oxidation of CH_4 (Z_{cl}) as a source of CO are included in Y_{ox}. We also consider the oxidation of Y to X as a source X to be negligible in this analysis.

In this study, we adopt the following three main methods to derive enhancement ratios:

Method (1): regression of the abundances (i.e., associated linear slope from the scatter plots between C_X and C_Y, C_X and C_Z, or C_Y and C_Z). This method is denoted as Bulk Enhancement Regression Ratio (BERr) (Andreae et al., 1988a; 1988b; Lefer et al., 1994; Silva et al., 2013; Tang et al., 2019) - See Eq. (5), Eq. (6) and Eq. (7).

Method (2): ratio of C_{spc} anomalies (Anomaly Enhancement Ratio or AERa) (Andreae and Merlet, 2001; Silva and Arellano, 2017; Le Canut et al., 1996) – See Eq. (8), Eq. (9) and Eq. (10).

Method (3): regression of C_{spc} anomalies (Anomaly Enhancement Regression Ratio or AERr) (Mauzerall et al., 1998; Yokelson et al., 2013; Hobbs et al., 2003; Wunch et al., 2009; Hedelius et al., 2018; Sim et al., 2022) – See Eq. (11) & Eq. (12).

The regressions and anomaly of abundances are calculated using daily average data points across a monthly time window. The number of daily column abundance data points available in each month at the selected TCCON location sites is provided in Figure S1. This information is used further in the analysis for selecting the data range for comparison purposes and interpreting the results.

Method 1: The enhancement ratio based on the regression of the daily average abundances of the species is considered as the "bulk" or "global" enhancement ratio (BERr), which is interpreted to represent the sum of all the associated sources and sinks contributions. The BERr or regression slope of daily average abundances of species X and Y for example is calculated simply as the ratio of the covariance of C_X and C_Y to the variance of C_X from a least-squares linear fit of the data. That is,

$$\left(\frac{\Delta C_Y}{\Delta C_X}\right)_1 = \frac{cov\,(C_Y, C_X)}{var(C_X)} \quad (5)$$

$$= \sum \frac{cov(X_{bg}, C_Y)}{var(C_X)} + \sum \frac{cov(X_{sources}, C_Y)}{var(C_X)} - \sum \frac{cov(X_{sinks}, C_Y)}{var(C_X)} \quad (6)$$

where sources of $X = ff, bb, c, r$ and sinks = p, o, st while subscript 1 denotes Method 1.

Note that for different linear regression approaches, there is a significant difference in the slope estimation when the representation of the error ($\epsilon_{meas,spc}$) associated with the data is included (Wu and Yu, 2018). To account for the differences in the estimates due to the choice of algorithm, we use three regression methods (Ordinary Least Squares, Geometric Mean and York) (York et al., 2004) in calculating the enhancement ratios derived based on regression approaches in Methods (1) and (3). The enhancement ratios of BERr and AERr reported in the study are the mean of these estimates weighted by the associated error (Verhulst et al., 2017).

$$BERr = \left(\frac{BERr_{OLS}}{\sigma^2{}_{OLS}} + \frac{BERr_{GM}}{\sigma^2_{GM}} + \frac{BERr_{York}}{\sigma^2_{York}}\right)\left(\frac{\sigma^2_{OLS}\sigma^2_{GM}\sigma^2_{York}}{\sigma^2_{OLS}\sigma^2_{GM}+\sigma^2_{OLS}\sigma^2_{York}+\sigma^2_{GM}\sigma^2_{York}}\right) \quad (7)$$

where BERr is the bulk enhancement ratio (or the weighted average of the slopes calculated from three regression algorithms). The weights are based on the associated errors (σ) from each regression algorithm.

Method 2. Local enhancement ratios are derived based on Methods (2) and (3), where the background influences/transport components are removed from the total abundances used in Method (1) using two ways to estimate anomalies (Eq 8). That is, 1) we remove dilution/boundary layer influence from the total abundance (broadly denoted as $C_{bg,spc}$) by taking the difference of average morning values from the average afternoon values (Wunch et al., 2009; Yokelson et al., 2013); and 2) we remove the 'background' by calculating the difference between the background value $C_{bg,spc}$ (assumed here as 5th percentile of the daily data) from the individual daily average values. Using the difference between morning and afternoon values of the abundance minimizes 1) the influence of high concentration of the species within the boundary layer in the morning (Yokelson et al., 2013); and 2) spectroscopic errors

(Wunch et al., 2009). The anomaly of C_{spc} after removing these influences from the total abundance is expressed as,

$$C'_{spc} = \left(C_{spc} - C_{bg,spc}\right) = \sum C_{sources} + \sum C_{sinks} \quad (8)$$

with AERa between species X and Y for Method (2) for example is given by:

$$\left(\frac{\Delta C_Y}{\Delta C_X}\right)_2 = \left(\frac{C'_Y}{C'_X}\right) = \frac{\sum Y_{sources} + \sum Y_{sinks}}{\sum X_{sources} + \sum X_{sinks}} \quad (9)$$

The average AERa is the weighted average of AERa calculated using the AERa from 1) boundary layer influence and 2) the 5th percentile methods. The weights are based on the errors (standard deviations) of C'_{spc} based on (1) and (2).

$$AERa = \left(\frac{AERa_1}{\sigma_1^2} + \frac{AERa_2}{\sigma_2^2}\right)\left(\frac{\sigma_1^2\sigma_2^2}{\sigma_1^2+\sigma_2^2}\right) \quad (10)$$

Method 3. Accordingly, the regression slope (AERr) between species X and Y for Method (3) for example can be calculated using the combination of Eqs. 5 and 8:

$$\left(\frac{\Delta C_Y}{\Delta C_X}\right)_3 = \frac{cov\,(C'_Y, C'_X)}{var(C'_X)} \quad (11)$$

$$= \sum \frac{cov(X'_{sources}, C'_Y)}{var(C'_X)} - \sum \frac{cov(X'_{sinks}, C'_Y)}{var(C'_X)} \quad (12)$$

The regression slopes are calculated using three algorithms as in Method 1 on the anomalies calculated from Method 2. AERr is the weighted average of the regression slopes and their associated errors similar to Eq. (7). Similar expressions can be applied to BERr, AERa, and AERr for species X and Z, as well as for Y and Z.

We also derive the enhancement of each species due to these regional and local enhancements. The regional enhancement ratio is calculated by subtracting the enhancement ratios derived based on the regression slope of total abundances in Method 1 (BERr) from that of the ratio derived from the anomalies in Method 3 (AERr) (Cheng et al., 2017; Briggs et al., 2016; Le Canut et al., 1996). The local enhancement ratio is given by AERr (from Method 3). Thus, the mean enhancement $(\overline{\Delta C_Y})_i$ of a species, Y for example, can be calculated as the product of $\left(\frac{\Delta C_Y}{\Delta C_X}\right)_i$ and C'_X, where i is either R=BERr-AERr or L =AERr, representing the regional (R) and local (L) enhancement ratio respectively and C'_X is the anomaly of species X calculated using Method 2 (AERa). That is, the regional (R) enhancement of CO for this example can be derived from the enhancement ratio in CO/CO_2 as: $\Delta C_{Y|X}{}^R = \left[\left(\frac{\Delta C_Y}{\Delta C_X}\right)_R \cdot C'_X\right]$ and similarly from the enhancement ratio in CO/CH_4 as: $\Delta C_{Y|Z}{}^R = \left[\left(\frac{\Delta C_Y}{\Delta C_Z}\right)_R \cdot C'_Z\right]$. We then take the mean of two enhancements ($\Delta C_{Y|X}{}^R$ and $\Delta C_{Y|Z}{}^R$) for species Y to account for species variations. Similar calculations are carried out for local (L) enhancements. The relative contribution of the regional and local enhancement ratio is calculated as $\frac{\text{BERr}-\text{AERr}}{\text{BERr}}$ and $\frac{\text{AERr}}{\text{BERr}}$ respectively.

3 Results and Discussion

This section describes the spatial and temporal variation and co-variation of C_{spc} along with their corresponding local and regional enhancement ratios. We also present in this section several qualitative inferences on the dominant processes leading to these co-variations.

3.1. Co-variation of CO, CO_2, and CH_4

From Figure S2, a clear seasonal cycle in XCO over all the locations in observed. This can indicate the presence of a non-steady state source/sink at the locations including potential regional transport into and out of the site. The seasonal cycle of X_{CO2} and X_{CH4} is evident for Pasadena, Garmisch, and Sodankylä based on the proximity of these sites to emission sources and sinks (e.g. carbon uptake by biosphere during summer) as described in Sect 2.1. The low seasonal cycles of CO_2 and CH_4 in other sites can be mainly due to its remote location with relatively mixed air masses and smaller influences of local emissions (e.g., Ciais et al., 2019).

Table 2: Mean and standard deviation, trend, amplitude, and co-variation of CO (ppb), CO_2 (ppm), and CH_4 (ppm) over the 11 TCCON sites. The correlations between the species are shown using a linear (Pearson's correlation) and a non-linear (mutual information/MI) metric.

Locations	Pasadena	Ascension	Manaus	Garmisch	Sodankylä	Anmyeondo	Burgos	Hefei	Darwin	Wollongong	Reunion
X_{CO}	93.5 ±11.5	84.4 ±10.3	94.0 ±12.0	86.4 ±9.1	88.5 ±11.1	104.8 ±10.8	84.5 ±11.9	118.3 ±13.5	72.0 ±12.2	59.7 ±7.8	67.3 ±9.1
X_{CO2}	403.5 ±5.5	398.3 ±4.0	398.6 ±1.2	400.5 ±6.0	399.6 ±6.7	403.3 ±3.8	406.8 ±1.9	404.5 ±2.8	397.8 ±5.1	397.4 ±5.1	397.8 ±4.5
X_{CH4}	1.83 ±0.02	1.81 ±0.01	1.83 ±0.01	1.82 ±0.02	1.81 ±0.02	1.85 ±0.01	1.85 ±0.02	1.88 ± 0.02	1.79± 0.02	1.77 ±0.02	1.78 ±0.01
Trend in X_{CO}	0.01 ±0.22	3.51 ±0.43		-0.00 ±0.14	-0.53 ± 0.22	-0.31 ±1.64			-0.98 ±0.64	0.27 ±0.35	-0.20 ±0.41
Trend in X_{CO2}	0.68 ±0.01	0.60 ±0.01		0.66 ±0.01	0.69 ±0.02	0.81 ± 0.10			0.66 ±0.01	0.64 ±0.01	0.63 ±0.01
Trend in X_{CH4}	0.36 ±0.03	0.45 ±0.01		0.47 ±0.02	0.48 ±0.02	0.21 ±0.15			0.45 ±0.02	0.44 ±0.01	0.45 ±0.01
Seasonal amplitude X_{CO}	36.0 ±4.5	35.3 ±3.1		33.2 ±8.5	37.2 ±3.9	16.4 ±0.0	27.4 ±15.5	38.3 ±0.0	33.7 ±10.2	33.2 ±8.5	33.7 ±9.2
Seasonal amplitude X_{CO2}	4.7 ±1.3	3.6 ±1.9		4.6 ±1.2	4.6± 1.4	3.6 ±0.0	4.6 ±1.4	5.6 ±0.0	4.4 ±1.4	4.6 ±1.2	4.4 ±1.3
Seasonal amplitude X_{CH4}	0.03 ±0.01	0.03 ±0.01		0.03 ±0.01	0.03 ±0.00	0.01 ±0.00	0.02 ±0.01	0.03 ±0.00	0.03 ±0.01	0.03 ±0.01	0.03 ±0.01
Correlation of X_{CO}:X_{CO2}	0.11	0.44	-0.66	0.12	0.19	0.29	0.42	0.41	0.03	0.13	0.20
MI of X_{CO}:X_{CO2}	0.11	0.18	0.39	0.27	0.42	0.48	0.30	0.35	0.19	0.16	0.17
Correlation of X_{CH4}:X_{CO2}	0.62	0.88	0.36	0.75	0.52	-0.04	-0.03	-0.13	0.93	0.80	0.88
MI of X_{CH4}:X_{CO2}	0.30	0.68	0.19	0.55	0.46	0.55	0.22	0.37	1.00	0.54	0.73
Correlation of X_{CO}:X_{CH4}	0.20	0.48	-0.05	-0.06	-0.19	0.18	0.38	0.23	0.1	0.39	0.26
MI of X_{CO}:X_{CH4}	0.11	0.17	0.39	0.16	0.24	0.36	0.42	0.31	0.12	0.17	0.10

To elucidate the dependence of similar variations and/or similar sources of origin, we show in Figure 2 the joint probability density distribution (PDF) between X_{CO} and X_{CO2}, X_{CO} and X_{CH4}, as well as X_{CO2} and X_{CH4}. We provide estimates of the associated dependencies (linear vs non-linear) among these species for the period listed in Table 2. The linear relationship is quantified using the Pearson's correlation while the non-linear dependency is estimated using mutual information (Kraskov et al., 2004). Consistent correlations across all three species suggest a similar source of origin, seen in the strong linear correlation across the species in Ascension and strong non-linear correlation across the species in Anmyeondo and Hefei. Strong dependencies are observed among X_{CO2} and X_{CH4} in most locations, where the correlations are higher than the ones between X_{CO} and X_{CO2} and X_{CO} and X_{CH4}. This is also seen in the joint distributions where the relationship between X_{CO2} and X_{CH4} is more apparent compared to others and point towards a shared signature from biospheric/natural and anthropogenic activities leading to a strong relationship between X_{CO2} and X_{CH4}. The differences observed between the non-linear and linear dependencies highlight the complexity of the relationship between the species and can be associated with the presence of daily variation in the sources and sinks, seasonality, differences in the lifetime of the species, as well as changes in the background present in the entire analysis period. We further investigate the variations in corresponding enhancement ratios in the next section to understand these differences.

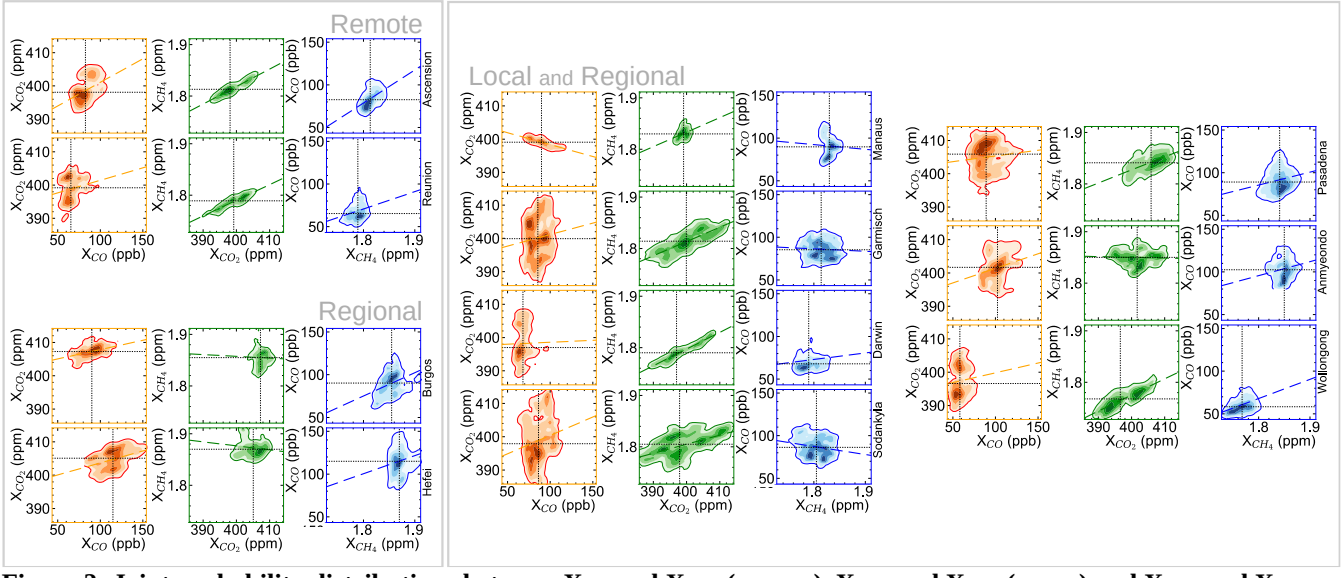

Figure 2: Joint probability distributions between X_{CO} and X_{CO2} (orange), X_{CO2} and X_{CH4} (green) and X_{CH4} and X_{CO} (blue) using daily values across 11 TCCON sites chosen for this study. The sites are grouped according to the site type and source influence on the species in these regions. X_{CO} is shown in ppb, whereas X_{CO2} and X_{CH4} have units in ppm. The straight lines denote the best-fit line from linear regression.

3.2. Enhancement Ratios of X_{CO}, X_{CO2}, and X_{CH4}

Figure 3 shows the mean variation of these enhancement ratios in X_{CO}/X_{CO2}, X_{CH4}/X_{CO2} and X_{CO}/X_{CH4}. Note that these ratios are calculated monthly across the daily data based on the methods explained in Sect. 2.2. The bulk enhancement ratio (BERr), which accounts for the total emission sources, sinks, and other contributions to observed abundances, is higher for all species in all measurement sites in comparison to the local enhancement ratios (AERa and AERr). Regionally, BERr in X_{CH4}/X_{CO2} is maximum over the Southeast Asian region (Anmyeondo, Burgos and Hefei) followed by the sites in SH (Darwin, Wollongong, Reunion, Ascension) when compared to other NH sites. This higher value of BERr in Southeast Asian region follows the regional maximum of X_{CO} and X_{CO2} described in Sect. 3.1 and shown in Figure S3. Similar is the case for the regional site variation of BERr in X_{CO}/X_{CH4}. The value of X_{CH4}/X_{CO2} from BERr is highest over Burgos and Wollongong followed by Garmisch, Sodankylä, Anmyeondo, and Pasadena. Relative differences can be observed between the correlations across the species and BERr suggesting more complex mixtures of the sources and sinks of these species at these sites.

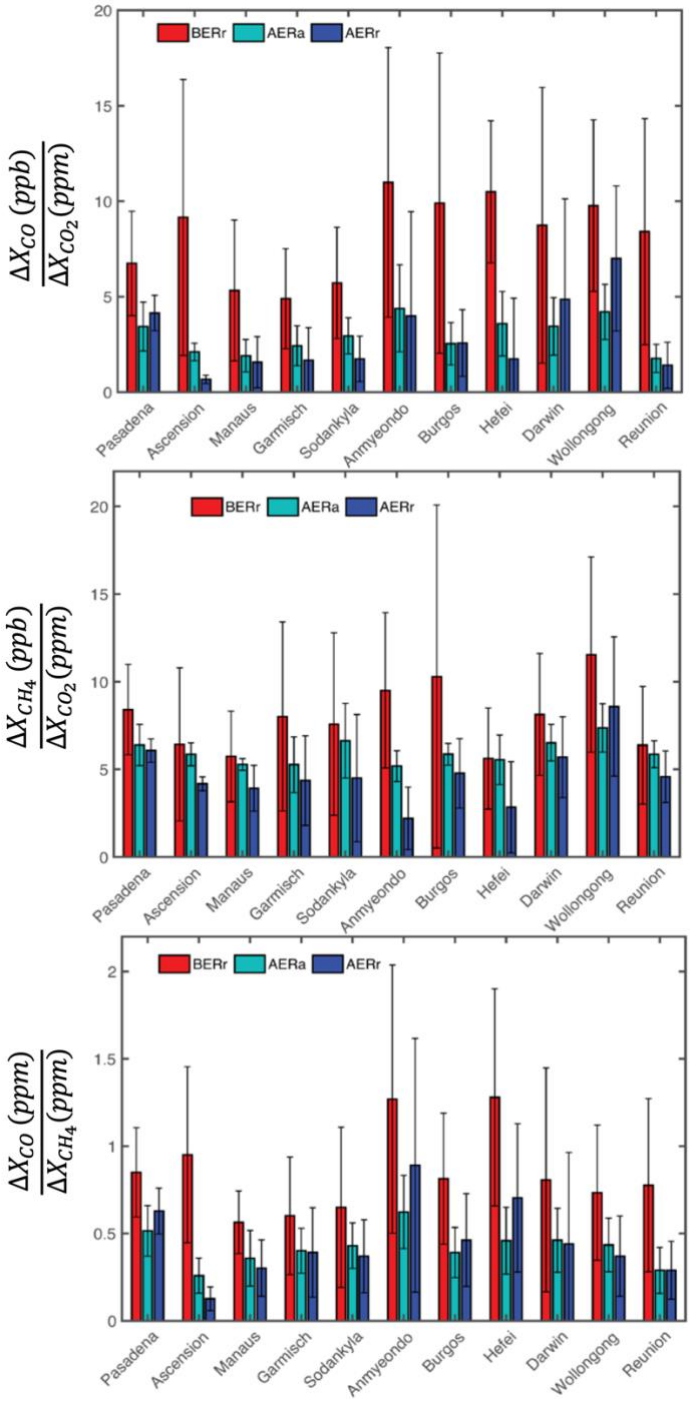

Figure 3: Mean variation of enhancement ratios calculated as Bulk Enhancement Ratio (BERr), Anomaly Enhancement Ratio (AERa), and Anomaly Enhancement Regression Ratio (AERr) of X_{CO}/X_{CO2}, X_{CH4}/X_{CO2} and X_{CO}/X_{CH4} during 2012-2019 over the 11 TCCON sites.

We note that the enhancement ratios derived in this work is within the range of ratio estimates reported in literature (Wunch et al., 2009; Wennberg et al., 2012; Silva et al., 2013; Buchholz et al., 2016; Hedelius et al., 2018; Bukosa et al., 2019). In Pasadena, Silva et al. (2013) reported an enhancement ratio in CO/CO_2 of about 9.3 -13.5 ppb/ppm based on MOPITTv5 and ACOS2.9/GOSAT CO_2 data, while Wunch et al. (2009) and Wennberg et al. (2012) reported 11 ppb/ppm and 8.4 ppb/ppm, respectively, along with the more recent study by Hedelius et al. (2018) which reported 7.1 to 7.5 ppb/ppm. Buchholz et al. (2016) and Bukosa et al. (2019) reported a range of ratios of about 1.3-37.4 ppb/ppm in CO/CO_2, 9.8-61 ppb/ppm in CH_4/CO_2 and 0.3-13 ppb/ppb in CH_4/CO over Australia. While generally consistent, our estimates also show that the range of ratios reported in these studies can vary (as can be expected) depending on the dominant processes (natural and/or anthropogenic) driving species abundance.

3.3. Regional and Local Contributions.

Additionally, the differences in the enhancement ratio from BERr, AERa, and AERr in Figure 3 can be indicative of different regional and local influences. As described in Sect. 2.2, the enhancement ratio calculated from the regression slope of the anomalies (AERr) represents a local enhancement ratio, where the associated regional enhancement ratio can then be derived by subtracting AERr from BERr (i.e., regional=bulk – local). Figure 4 shows the average seasonal variation of the regional (BERr - AERr) and local enhancement ratios (AERr) for each species. This reveals how the contribution and influence of regional and local enhancement ratios in the bulk ratio vary seasonally. The seasonal variations calculated for DJF should read as Winter in NH and Summer in SH, MAM months as Spring in NH and Fall in SH, JJA months as Summer in NH and Winter in SH and SON months as Fall in NH and Spring in SH. The corresponding number of months available to generate the average seasonal variation of regional and local enhancement ratio is provided in supplementary material (Table S1 and S2). Note that for sites like Sodankylä, there are only 4 data points for seasonal averaging during winter months due to limited measurements during this period.

We see in Figure 4 that the seasonal variation of regional and local enhancement ratios at different measurement sites reveals the presence of seasonally varying driving factors in the bulk enhancement ratios. The local enhancement ratio appears to dominate over the regional ratios for Pasadena across all seasons. The local enhancement ratios in X_{CO}/X_{CO2} and X_{CO}/X_{CH4} compared to the regional ratios are more significant during Fall season (SON). This may be due to the poor dependency between transported CH_4 or CO_2 coming from biospheric sources or any non-combustion sources of CO. This is evident in Figure S3 which shows a significant peak in the abundance of X_{CO2} during Fall months over Pasadena, but not in X_{CO}. Furthermore, the low value of regional enhancement ratio in X_{CH4}/X_{CO2} during Summer over Pasadena may be associated with the poor correlation among the species from independent sources or from biospheric sinks of CO_2 (see Tables S1 and S2). Similar seasonal variation is observed at Wollongong where it shows a dominant influence of local enhancements of species ratios for most of the seasons. Relative to the regional ratio, the magnitude of local enhancement ratio in X_{CH4}/X_{CO2} is more significant during the months of DJF, which is the summer season in SH. The seasonal variation of X_{CO}/X_{CH4} follows a different pattern in Wollongong with the regional influence

dominating for all seasons except JJA (winter in SH). This can be attributed to similar chemical loss of CO and CH_4 through OH especially in spring and summer in SH (Lelieveld et al., 2016; Fisher et al., 2015). The seasonal variation of species enhancement ratio in X_{CH4}/X_{CO2} and X_{CO}/X_{CH4} at Darwin follows similar variations as that in Wollongong although there are differences in absolute magnitude due to seasonal bushfire occurrences and fire emissions across south and north Australia. The regional enhancement ratio in X_{CO}/X_{CO2} dominates during DJF (summer) and SON (spring) months at Darwin whereas the local enhancement ratio dominates in other seasons. A large difference of about 10 ppb/ppm is also observed between local and regional enhancement ratio in X_{CO}/X_{CO2} during JJA (winter) months.

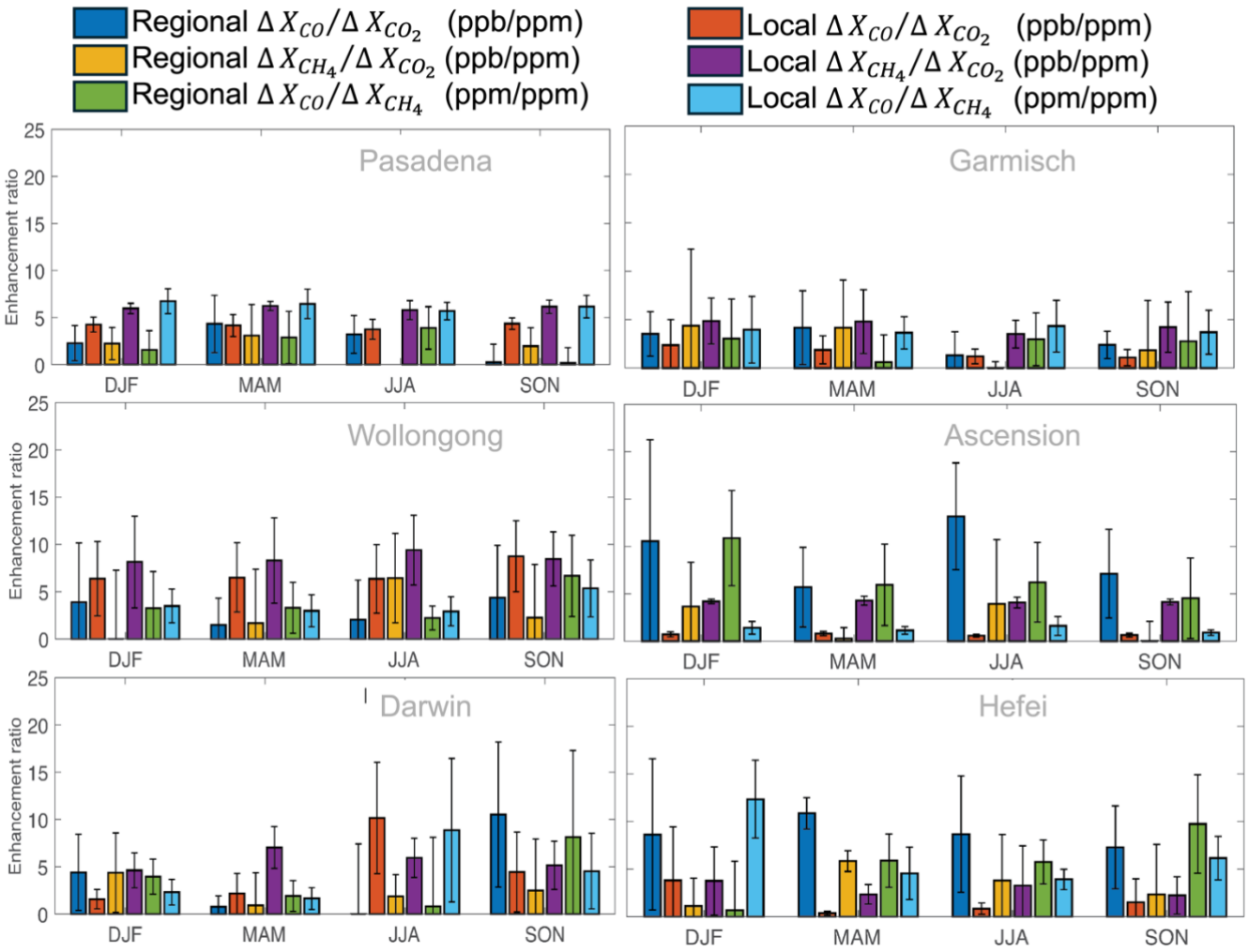

Figure 4: Average seasonal variation of regional and local enhancement ratio in CO/CO_2, CH_4/CO_2 and CO/CH_4 during 2012-2019 over Pasadena, Garmisch, Wollongong, Ascension, Darwin, and Hefei.

Furthermore, in Ascension, the influence of regional enhancement ratios in X_{CO}/X_{CO2} and X_{CO}/X_{CH4} is high during all seasons whereas the seasonal variation in X_{CH4}/X_{CO2} shows a different pattern. Except in Spring (SON) and Fall (MAM), the seasonal influence of the regional and local enhancement ratio in X_{CH4}/X_{CO2} is comparable. The low values of regional enhancement in X_{CH4}/X_{CO2} during Spring and Fall may be associated with the poor correlation among the species from independent sources or from biospheric sources of CO_2. The seasonal variation of enhancement ratio at Manaus and Reunion follows this characteristic as well (shown in Figure S4). The relative importance of regional and local enhancement ratio varies among species in Garmisch and Sodankylä (in Figures S3). The regional enhancement ratio in X_{CO}/X_{CO2} and local enhancement ratio in X_{CO}/X_{CH4} ratio dominate for all seasons at Garmisch (Figure 4) and Sodankylä (Figure S4) while the local enhancement ratio in X_{CH4}/X_{CO2} dominates during JJA (winter) and SON (spring) months compared to other seasons over these sites. Finally, irrespective of the season, regional enhancements in X_{CO}/X_{CO2} dominate at Hefei and Burgos (Figure S4) while the same is true in X_{CH4}/X_{CO2} at Anmyeondo (Figure S4). The local enhancement ratio in X_{CH4}/X_{CO2} and X_{CO}/X_{CH4} dominates only during DJF (winter) at Hefei, while local enhancement ratio in X_{CO}/X_{CH4} dominates for all seasons at Anmyeondo except fall (SON). The local enhancement ratio in X_{CO}/X_{CH4} also dominates regardless of season at Burgos.

The average relative contribution of local and regional enhancement ratio towards the bulk enhancement ratio at each measurement site is provided in Table 3. A clear difference is observed in the contribution of the local and regional enhancement ratios across each measurement site and among species. Locations like Pasadena and Wollongong show the dominant local influence for X_{CO}/X_{CO2} whereas the rest of the locations report significant regional influences. This regional contribution in X_{CO}/X_{CO2} to the bulk enhancement ratio is highest over Ascension followed by Burgos (>80%). This can be attributed to the fact that Ascension is a remote location and the sharp rise in the column abundance of CO at Ascension can be associated to a rise in transported CO from the nearby African region. Previous studies over Burgos and vicinity also reported enhanced CO and CH_4 due to transport of emissions from East Asia (Velazco et al., 2017; Hilario et al., 2021). This inference is in support of the location features provided in Sect. 2.1 and source information as reported in previous studies. The contribution of regional enhancement ratios dominates over Manaus, Anmyeondo, Sodankylä, Hefei and Burgos to the bulk enhancement ratio in X_{CH4}/X_{CO2} while the remaining sites report dominance of its local enhancement ratio. Except for Ascension, Manaus, Darwin, Anmyeondo, and Reunion, the contribution of local enhancement ratio in X_{CO}/X_{CH4} is higher than the regional at all other measurement sites.

With the difference in the contributions of regional and local enhancement ratios, we also derive the enhancement of each species due to these regional and local enhancements as outlined in Sect. 2.2. The average variation of the regional and local enhancements of X_{CO}, X_{CO2}, and X_{CH4} is provided in Figure S5. A large difference (10-28 ppb) is observed in the relative increase of X_{CO} between regional and local enhancements over Burgos, Ascension, and Reunion. The relative increase of X_{CO2} at Sodankylä, Anmyeondo, and Burgos show dominance of local enhancements while the remaining locations show higher importance of regional processes. Except at Ascension and Anmyeondo, all other measurement sites show that the relative rise in X_{CH4} comes from regional processes. The difference in relative increase in X_{CO2} and X_{CH4} between regional and local enhancements is less in most of the locations

compared to the corresponding relative increase in X_{CO}. This smaller difference in the relative increase can be attributed to the long lifetime, uniform mixing characteristic and the large background value of X_{CO2} and X_{CH4} compared to that of X_{CO} in the atmosphere. The different process or source types leading to this regional variation and seasonality in the local and regional enhancement ratio is further analyzed using the scatterplots of multiple species ratios in the next section.

Table 3: Percent contribution of regional and local enhancements and their associated errors to the ratio of X_{CO}/X_{CO2}, X_{CH4}/X_{CO2} and X_{CO}/X_{CH4} during 2012-2019 over the 11 TCCON sites.

	X_{CO}/X_{CO2}				X_{CH4}/X_{CO2}				X_{CO}/X_{CH4}			
	Local (%)		Regional (%)		Local (%)		Regional (%)		Local (%)		Regional (%)	
Location	μ	σ	μ	σ	μ	σ	μ	σ	μ	σ	μ	σ
Pasadena	63.09	13.83	36.91	26.78	72.23	8.01	27.77	22.68	71.04	15.44	28.96	14.65
Ascension	11.99	2.41	88.01	76.66	59.96	6.09	40.04	61.95	16.65	7.15	83.35	45.86
Manaus	32.34	25.22	67.66	44.1	44.57	22.7	55.43	22.56	48.51	28.6	51.49	4.06
Garmisch	33.46	34.97	66.54	19.14	50.64	31.89	49.36	35.4	51.78	42.61	48.22	13.41
Sodankylä	30.43	20.82	69.57	30.13	41.65	47.91	58.35	20.74	52.84	32.13	47.16	38.56
Anmyeondo	29.35	49.77	70.65	15.5	19.92	18.72	80.08	28.13	40.84	57.25	59.16	4.38
Burgos	14.37	17.7	85.63	61.79	41.17	19.36	58.83	75.98	51.53	32.66	48.47	13.5
Hefei	27.28	30.28	72.72	8.75	49.97	46.25	50.03	7.01	51.22	33.21	48.78	15.45
Darwin	41.05	60.27	58.95	22.48	59.14	28.44	40.86	14.42	41.83	64.86	58.17	15.01
Wollongong	59.64	38.88	40.36	7.27	58.94	34.45	41.06	13.83	46.11	31.38	53.89	21.46
Reunion	24.56	14.37	75.44	56.13	58.35	23	41.65	29.73	41.93	21.33	58.07	42.54

3.4. Inferring dominant process contribution from multi-species enhancement ratios

Figure 5 shows the scatter plot of the ratio in X_{CO}/X_{CO2} vs X_{CO}/X_{CH4} and X_{CH4}/X_{CO2} vs X_{CH4}/X_{CO} for regional and local enhancements. We use the relationship of the multi-species ratios (X_{CO}/X_{CO2} vs X_{CO}/X_{CH4} and X_{CH4}/X_{CO2} vs X_{CH4}/X_{CO}) to qualitatively infer the processes influencing the regional and local enhancements ratios at each measurement site. For example, high temperature/more-efficient combustion processes lead to the emission of more CO_2 compared to CO and low-temperature combustion produces more CO (Silva and Arellano, 2017). Similarly, activities associated with the extraction of coal, and distribution of natural gas, wetland, rice cultivation, landfill, and livestock result in higher emission of CH_4 compared to emissions of CO and CO_2. Lower (higher) ratio values of both X_{CO}/X_{CO2} vs X_{CO}/X_{CH4} in the scatter plots can be related to processes emitting lower (higher) CO. Similar approach is applied for ratio variations in X_{CH4}/X_{CO2} vs X_{CH4}/X_{CO}. We confirm the classification of these low to high values using K-means clustering. A summary of these categories for both regional and local enhancements are listed in Table 4 and 5.

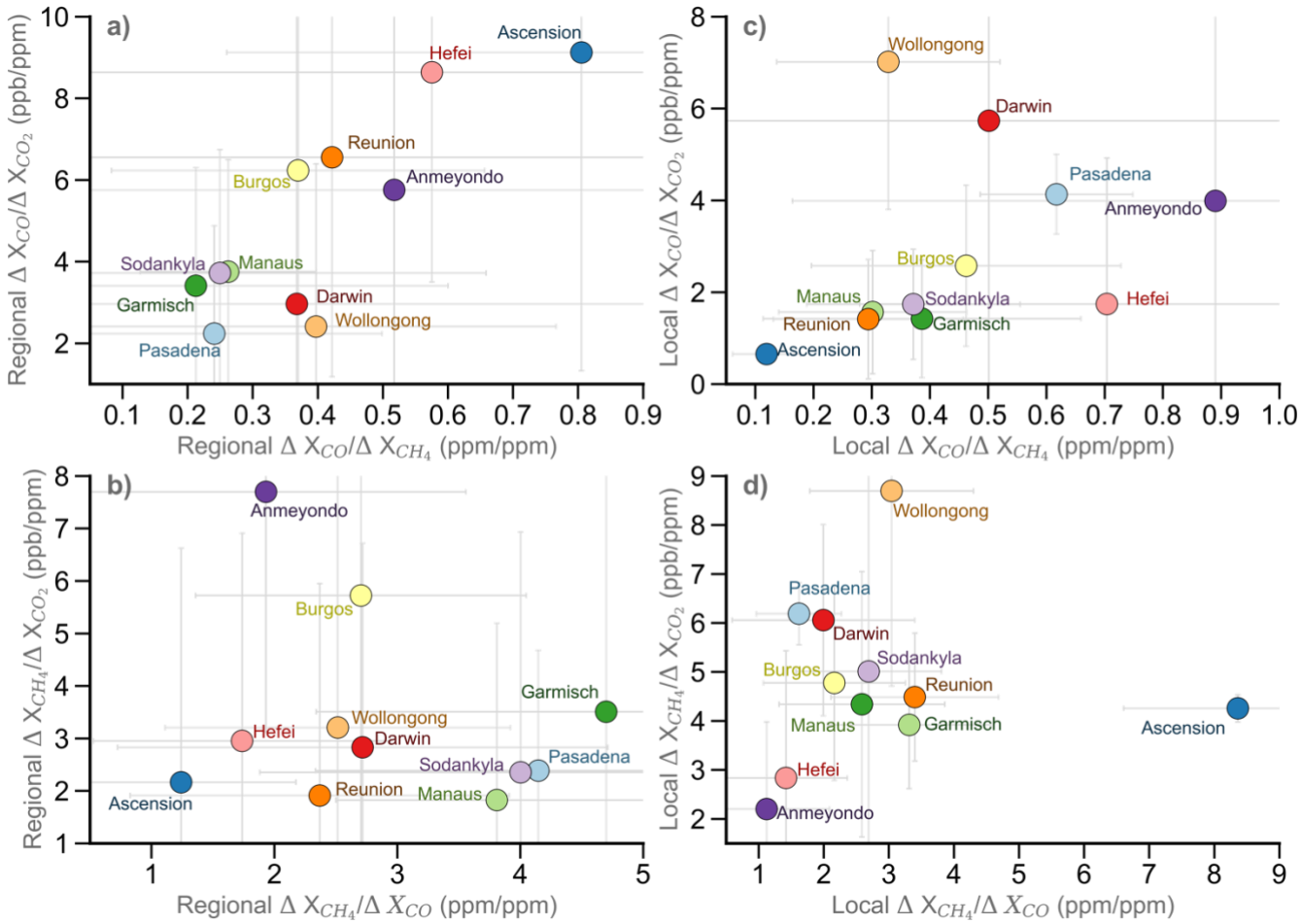

Figure 5: Scatter plot of average regional (left column) and local (right column) enhancement ratios in CO/CO_2 vs CO/CH_4 (top row) and CH_4/CO_2 and CH_4/CO (bottom row) during 2012-2019 with their associated errors.

The scatter plot of regional enhancement ratio of species at Pasadena, Manaus, Garmisch, Sodankylä, Darwin, and Wollongong show relatively low value of X_{CO}/X_{CO2} vs X_{CO}/X_{CH4} and medium/high value of X_{CH4}/X_{CO2} vs X_{CH4}/X_{CO}. The regional enhancement ratio showed a value between 2.24 and 3.75 ppb/ppm for X_{CO}/X_{CO2}, between 1.83 to 3.51 ppb/ppm for X_{CH4}/X_{CO2} and 3.81 to 4.69 ppm/ppm for X_{CH4}/X_{CO} over these regions. This pattern can suggest a dominant process (or a combination of) that is characterized by low CO and high CH_4 and/or CO_2 emissions from natural and biospheric sources, and/or anthropogenic sources with high activity and efficiency. These values fall within the range of previously reported ratios for a mixture of natural and anthropogenic emissions (2-6 ppb/ppb for X_{CH4}/X_{CO2} and 3.3-8.0 ppb/ppm for X_{CO}/X_{CO2}, Bukosa et al., 2019). The location features of these measurement sites provided in Sect. 2.1 also support this result.

Table 4: Regional process inference based on the ratio of X_{CO}/X_{CO2} vs X_{CO}/X_{CH4} and X_{CH4}/X_{CO2} and X_{CH4}/X_{CO} over the 11 TCCON sites.

Regional	X_{CO}/X_{CO2}		X_{CO}/X_{CH4}		X_{CH4}/X_{CO2}		X_{CH4}/X_{CO}		Regional Process/Source Type
Location	μ	σ	μ	σ	μ	σ	μ	σ	
Pasadena	2.24	0.12	0.24	1.81	2.38	1.91	4.15	1.81	Biogenic/biospheric and some combustion
Ascension	9.12	0.44	0.81	7.02	2.16	3.98	1.24	0.93	Combustion processes (fires)
Manaus	3.75	0.02	0.26	2.35	1.82	1.29	3.81	1.31	Biogenic/Biospheric and some combustion
Garmisch	3.41	0.08	0.21	0.94	3.51	2.84	4.7	2.36	Biospheric/Wetland [or other CH_4 sources]
Sodankylä	3.72	0.25	0.25	1.73	2.35	1.57	4	2.12	Biospheric/ Wetland [or other CH_4 sources]
Anmyeondo	5.76	0.06	0.52	1.7	7.7	2.67	1.93	1.63	High temp combustion/Bio-fuel combustion
Burgos	6.23	0.11	0.37	6.12	5.72	7.82	2.7	1.34	Biofuel, coal/some combustion
Hefei	8.64	0.2	0.58	0.92	2.95	0.39	1.74	1.21	Low temp combustion (biomass burning)
Darwin	2.96	0.12	0.37	1.97	2.83	1.17	2.72	1.99	Biospheric or fires (mixed)
Wollongong	2.41	0.16	0.4	0.71	3.21	1.6	2.52	1.40	Biogenic, Bio-fuel combustion (or mixed)
Reunion	6.55	0.33	0.42	4.72	1.91	1.9	2.37	1.54	Biospheric/Combustion

Table 5: Local process inference based on the ratio of X_{CO}/X_{CO2} vs X_{CO}/X_{CH4} and X_{CH4}/X_{CO2} and X_{CH4}/X_{CO} over the 11 TCCON sites.

Local	X_{CO}/X_{CO2}		X_{CO}/X_{CH4}		X_{CH4}/X_{CO2}		X_{CH4}/X_{CO}		Regional Process/Source Type
Location	μ	σ	μ	σ	μ	σ	μ	σ	
Pasadena	4.13	0.13	0.62	0.93	6.19	0.67	1.62	0.65	Biogenic/ Bio-fuel combustion (or fires)
Ascension	0.65	0.07	0.12	0.22	4.26	0.39	8.36	1.75	Non-combustion
Manaus	1.57	0.16	0.3	1.34	3.92	1.3	3.31	1.26	Biogenic/Biospheric or other combustion
Garmisch	1.42	0.26	0.39	1.71	4.34	2.56	2.59	1.27	Biospheric/Biogenic fires
Sodankylä	1.74	0.21	0.37	1.19	5.01	3.64	2.69	1.12	Biospheric/Remote
Anmyeondo	3.99	0.73	0.89	5.47	2.2	1.78	1.12	0.97	Low temp combustion/ Biofuel combustion
Burgos	2.57	0.27	0.46	1.75	4.78	1.99	2.16	1.09	Biospheric and some combustion
Hefei	1.74	0.42	0.7	3.18	2.84	2.6	1.42	0.94	Low temp combustion/Biofuel
Darwin	5.73	0.52	0.5	5.27	6.06	2.31	1.99	1.40	Biospheric and some combustion
Wollongong	7.02	0.23	0.33	3.8	8.69	3.98	3.04	1.26	Biogenic, Bio-fuel combustion (or fires)
Reunion	1.41	0.17	0.29	1.21	4.49	1.47	3.39	1.29	Biospheric/ Biogenic fires

A relatively high/medium value of X_{CO}/X_{CO2} (6.55-9.12 ppb/ppm) vs X_{CO}/X_{CH4} ratio and relatively low value of X_{CH4}/X_{CO2} (1.91-2.95 ppb/ppm) vs X_{CH4}/X_{CO} (1.24-2.37 ppb/ppm) ratio can be seen in Reunion, Ascension, and Hefei. This variation appears to suggest the presence of low-temperature combustion processes (i.e., biomass burning especially smoldering fires) emitting more CO. A study by Bremer et al. (2004) attributed the enhancement in MOPITT-based CO column abundance at Ascension to Sub-Saharan biomass burning emissions while Zhou et al., 2018) reported that the seasonality of CO at two sites, St Denis and Maido (in Reunion), is primarily driven by biomass burning emissions in Africa and South America. Wang et al., 2017 also reported an enhancement ratio of 5.6 ppb/ppm for X_{CO}/X_{CO2} at Hefei during October 2014 and recognized incomplete combustion of fossil-fuels as the main source of CO in this area. The relatively medium value of X_{CO}/X_{CO2} (5.76 and 6.23 ppb/ppm) vs X_{CO}/X_{CH4} and high X_{CH4}/X_{CO2} (7.69 and 5.72 ppb/ppm) vs X_{CH4}/X_{CO} (1.93 and 2.71 ppm/ppm) suggest the presence of fossil-fuel emissions, coal/biofuel processes, agriculture, or wetland emissions over Anmyeondo and Burgos. The ratio is close to the range of ratios of 3.3-8 ppb/ppm for X_{CO}/X_{CO2} and 1.6-4.2 ppb/ppb for X_{CH4}/X_{CO} reported in emissions of mixed anthropogenic sources from rural and urban areas (Bukosa et al., 2019). Initial analysis of TCCON data in Burgos by Velazco et al. 2017 suggested that the enhancement in CO over the northern part of the Philippines is mostly from fossil-fuel emissions, which is dominated by transported emissions from East Asia, and have little influence from biomass burning, which can be large over the southern part of the region (Edwards et al., 2022).

The scatter plot of local enhancement ratio over Wollongong conveys a relatively high/medium ratio in X_{CO}/X_{CO2} (7.02 ppb/ppm) vs X_{CO}/X_{CH4} and relatively high/medium ratio in X_{CH4}/X_{CO2} (8.69 ppb/ppm) vs X_{CH4}/X_{CO} (3.04 ppm/ppm). This appears to suggest active low-temperature combustion (biomass burning or fires) producing CO and biofuel combustion or coal activities leading to the production of more CH_4. This value is within the range of values reported for mixed anthropogenic emissions in Wollongong (Buchholz et al., 2016). Our estimated value is less than the ratio of 13-61 ppb/ppm in X_{CH4}/X_{CO2} reported in Wollongong for coal mining. This may be due to the impact of mixing (dilution) of other sources. The ratio of 4.13 and 5.73 ppb/ppm in X_{CO}/X_{CO2}, 6.18 and 6.06 ppb/ppm in X_{CH4}/X_{CO2} and a lower ratio in X_{CH4}/X_{CO} (1.62 and 1.99 ppm/ppm) appears to suggest the presence of mixed emissions from anthropogenic or combustion activities in Pasadena and Darwin. This coincides with reports by Hedelius et al. (2018) of a canyon gas leak and wildfire activities based on a ratio of 7.3 ppb/ppm in CH_4/CO_2 and 7.1 ppb/ppm in X_{CO}/X_{CO2} in Pasadena. The local enhancement ratio at remaining locations shows a relatively low ratio in X_{CO}/X_{CO2} vs X_{CO}/X_{CH4} and relatively medium/high ratio in X_{CH4}/X_{CO2} vs X_{CH4}/X_{CO}, which can indicate dominance of biogenic or non-combustion processes influencing these ratios at these locations. The scatter plots of these enhancement ratios between species across seasons (Figures S6 to S9) reveal similar results shown in Figure 5, but slight seasonal variations are observed at Hefei, Reunion, Darwin, and Wollongong.

3.5. Comparison of column abundance with emission estimates.

We show in Figure 6 the average contribution (in %) to the emissions of CO, CO_2, and CH_4 over these measurement sites from the anthropogenic sector as reported in the Copernicus Atmosphere Monitoring Service emission inventory (CAMS v4.1, Granier et al., 2019), and biomass burning sector as reported

in the Global Fire Emission Database (GFED4, Giglio et al., 2013). These emission inventories are utilized for qualitative comparison of local emission sources or processes inferred from the scatterplot relationships of multi-species enhancement ratios (see Table 4 and 5). It has to be noted that most of the emissions from the anthropogenic sector of CAMS have emissions with less temporal variability compared to seasonal variability, including inter-annual variability of biomass burning emissions from GFED. The average total emissions around the grid location of the TCCON measurement site is also provided in Figure 6.

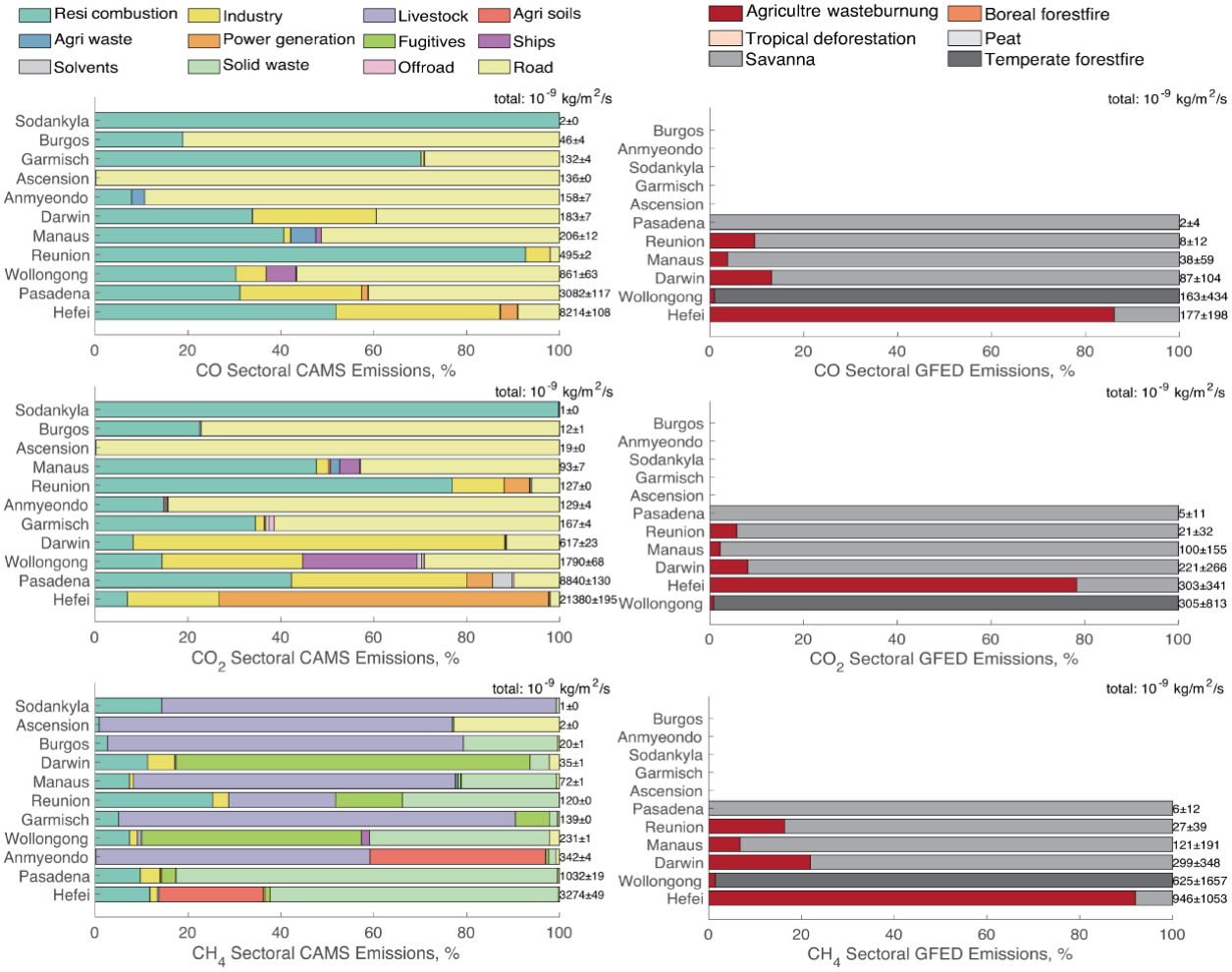

Figure 6: Sectoral emission distribution (%) of CO, CO_2, and CH_4 from CAMS anthropogenic emissions (left) and GFED fire (right) at TCCON measurement sites during 2012 - 2019. Corresponding total emissions are indicated in the secondary (right) y-axis.

Regionally, the anthropogenic and fire emission sectors dominate over Hefei, Wollongong, and Darwin compared to other sites (Figure 6). The anthropogenic emission sectors for CO, CO_2, and CH_4 are also significant over Hefei, Pasadena, Wollongong, and Anmyeondo. Residential combustion, industries, power generation, and road transport influence local CO at Hefei. Similarly, residential combustion, industries, and road transport influences local CO in Pasadena whereas in Wollongong CO emissions

come from only residential combustion and road transport sectors. A large portion of CO_2 emission in Hefei comes from the power generation sector followed by industries and residential combustion. The major CO_2 emission sectors in Pasadena include industry and residential combustion. Wollongong has CO_2 emissions from the following sectors: industry, residential combustion, and ships. Note that Hefei, Pasadena, Anmyeondo, and Wollongong have significant emissions of CH_4 from anthropogenic sectors. Solid waste, and agricultural soils are the significant emission sectors for CH_4 at Hefei. The main sectors for CH_4 emissions at Anmyeondo include livestock and agricultural soils. Emissions from fugitives, solid waste and water are significant emitters of CH_4 at Wollongong. These mixtures of emission sectors at these sites support the dominant processes identified in the previous section using the correlation of enhancement ratios of these species from TCCON (Figure 5, Table 4, and 5).

The emission from biomass burning is one of the main factors influencing the seasonality and inter-annual variability in the abundance of species. The strong monthly variability of CO and CO_2 at Darwin, Wollongong, Reunion, and Pasadena can be attributed to the seasonality of biomass burning emissions (Figure S2 and Figure 5). Agricultural waste burning is the main emission sector for CO, CO_2, and CH_4 at Hefei. The seasonality of CO, CO_2, and CH_4 at Wollongong is due to emissions from temperate forest fires (Figure 5) while the biomass burning activity at Darwin, Reunion, and Manaus appears to be dominated by savanna fires followed by agricultural waste burning (Figure 5). Sodankylä, Ascension, and Burgos sites are remote locations and surrounding (local) emissions are therefore smaller than that of the other sites. Even though Reunion Island is a relatively small and isolated island, contribution from local biomass burning activity and other anthropogenic sources is found to be considerable.

4 Summary and Future Directions

Despite the growing global burden in CO_2 and CH_4, current measurements of total column CO_2 (X_{CO2}) and CH_4 (X_{CH4}) provide a limited verifiable capability in identifying and quantifying specific types of their corresponding sources and sinks. In addition to the lack of vertical information from these column measurements, the diffusive nature of the atmosphere (mixing air masses influenced by spatially and temporally heterogenous sources and sinks), make it very challenging to track source type contributions to these observed column abundances. In this work, we combine simultaneous ground-based measurements of total column abundances of CO_2 and CH_4 with CO (X_{CO}) to further characterize the associated enhancements in the column abundance of the respective species by taking advantage of their temporal co-variations. A total of 11 sites from Total Carbon Column Observing Network (TCCON), including six stations in NH and five in SH, are selected to investigate associated multi-species patterns during 2012 to 2019 period. We also introduce a combination of established regression and anomaly approaches to derive mean local and bulk enhancement ratios between X_{CO}/X_{CO2}, X_{CO}/X_{CH4} and X_{CO2}/X_{CH4} across each month of daily data. We first derive "bulk" enhancement ratios (BERr) using 3 regression algorithms (ordinary least squares, geometric regression, York regression) where we report the BERr as the mean across these algorithms weighted by the associated errors. We also employ a "local" anomaly approach, where observed column abundances are pre-subtracted by assumed "background" values. These background values are derived as the mean of a) daily anomalies calculated

by subtracting the morning from afternoon columns; and b) 5th percentile of daily data. The enhancement ratios based on anomalies are derived either from monthly mean ratios (AERa) or regressed slope (AERr) between these anomalies. This combination of approaches allows us to not only account for the variability on our estimates of enhancement ratios due in fact from the algorithms and assumptions of background values, but also to separate the regional and local influences on these ratios by subtracting BERr ("bulk or global") from AERr or AERr ("local") estimates.

Our results show that: a) estimates of enhancement ratios are within the range of ratio estimates reported in literature; b) regional and local influences to these ratios can be disentangled with resulting values that appear to be physically reasonable relative to current understanding of process drivers at these site locations; and c) multi-species analysis of these enhancement ratios can augment current techniques aimed at characterizing dominant types of sources and sinks influencing observed abundances. We find that Pasadena (Wollongong, Manaus) shows a dominant (moderate) local influence (>60% in Pasadena, >50% in Wollongong and Manaus) across CO, CH_4, and CO_2 which appear to come from a mixture of biospheric and combustion activities. In contrast, Anmyeondo show a dominant regional influence (>~60%) across all species, which appear to come from high temperature and/or biofuel combustion activities. Comparable influence of regional and local enhancement is observed in Darwin (biospheric and/or low-temperature combustion) for all species. Interestingly, Sodankylä and Garmisch (mostly biospheric and wetlands), Hefei (low-temperature combustion) and Burgos (biofuel combustion) are characterized by larger regional influence (~67 for Garmisch, ~70% for Sodankylä, ~73% for Hefei and 86% for Burgos) in X_{CO}/X_{CO2} and relatively comparable regional and local influences in X_{CH4}/X_{CO2} and X_{CO}/X_{CH4}. On the other hand, Ascension shows a large regional influence (>80%) for both X_{CO}/X_{CO2} and X_{CO}/X_{CH4} indicative of fire activities (high CO). While Ascension is relative characterized as "remote" with little local influence in column CO, it appears to show the impact of long-range transported emissions (most likely fires). Note that total column CO (X_{CO}) can capture this fire signature as opposed to several reports over Ascension which have indicated that fire plumes from southern Africa cannot be observed from ground-based site in the island. Similar finding is observed in Reunion (albeit not as large regional influence, ~75% in X_{CO}/X_{CO2} and ~58% in X_{CO}/X_{CH4}). As with Ascension, Reunion is on an isolated island and characterized as "remote" but with large presence of combustion (fire) influence as it receives higher amounts of smoke outflows from African fires on its west and sometimes even South American fires. These results are qualitatively consistent with corresponding estimates from CAMS and GFED emission inventories. We do however want to note that additional work is needed for a more robust estimation of the BERr and the regional enhancement, considering the high variability observed across the species in BERr (as in Figure 3) which consequently leads to higher variability in the regional enhancement estimates.

This work is envisioned to serve as one of the bases for interpreting enhancement ratios derived from current space-borne collocated column measurements of CO, CO_2, and/or CH_4 (e.g., TROPOMI, GOSAT-2, OCO-2, and OCO-3). The method presented here can also be applied to future geostationary satellites that will provide sub-daily measurements such as GeoCARB (e.g., Moore et al., 2018). Our method provides a preliminary framework towards the evaluation of the enhancement ratios (i.e., species sensitivities) along with the abundances derived from these satellite missions to reduce the discrepancies between the top-down and bottom-up inversions and emission-based studies, as well as to

provide more robust source type attribution of these abundances that otherwise is difficult to obtain by single species analysis alone. The use of enhancement ratios and their separation into regional and local influence allows us to effectively disentangle the source type and transport signatures of these species over the sites, unlike the correlation estimates in Table 2 which do not provide a complete picture considering the diffused (non-linear) behavior of their sources and sinks. Separating the contributions of megacity emissions from fire and biogenic sources is a future application of this study. Use of data-driven machine learning regression algorithms can also assist in inferring the contribution from different emission sources. Including additional sites and a longer time period from the newer software version of the TCCON data (GGG2020) will also aid in constraining the uncertainty of the regional versus local enhancements, and the source/transport signatures inferred in this study.

Acknowledgements

This research work is supported by NASA ACMAP Grant (80NSSC19K0947). Dr. Tang is supported by NCAR Advanced Study Program Postdoctoral Fellowship. The TCCON data for total column measurement of CO, CO_2 and CH_4 at Pasadena, Ascension, Manaus, Garmisch, Sodankylä, Anmyeondo, Burgos, Hefei, Darwin, Wollongong, and Reunion were obtained from the TCCON Data Archive hosted by CaltechDATA at https://tccondata.org. The TCCON site at Réunion Island has been operated by the Royal Belgian Institute for Space Aeronomy with financial support since 2014 by the EU project ICOS-Inwire (Grant agreement ID 313169), the ministerial decree for ICOS (FR/35/IC1 to FR/35/C6), ESFRI-FED ICOS-BE project (EF/211/ICOS-BE) and local activities supported by LACy/UMR8105 and by OSU-R/UMS3365 – Université de La Réunion. The Burgos TCCON site is supported in part by the GOSAT series project, with local support from the Energy Development Corp. Philippines. We also acknowledge the Emission of Atmospheric Compounds and Compilation of the Ancillary Data (ECCAD, https://eccad.sedoo.fr) for anthropogenic and biomass burning emission data of CO, CO_2, and CH_4 from the inventories of Copernicus Atmosphere Monitoring Service (CAMS v4.1) and Global Fire Emission Database (GFED4) during 2012-2019 period. This material is partly based upon work supported by National Center for Atmospheric Research, which is a major facility sponsored by the National Science Foundation under cooperative agreement no. 1852977.

Data Availability Statement

The TCCON data were obtained from the TCCON Data Archive hosted by CaltechDATA at https://tccondata.org, while the following supporting datasets were obtained from: Emission of Atmospheric Compounds and Compilation of the Ancillary Data (ECCAD, https://eccad.sedoo.fr/) for CAMS v4.1 and GFED4; MOPITT from NASA through the Earthdata portal (https://earthdata.nasa.gov), GOSAT-1 from NIES at https://data2.gosat.nies.go.jp, and OCO-2 from NASA through the Goddard Earth Science Data and Information Services Center (https://disc.gsfc.nasa.gov/datasets?keywords=l3co2) for registered users.

Author Contribution

Conceptualization: AFAJ, WT; Investigation: KM, VB, CR, and AFAJ; Methodology: KM, VB, AFAJ, CR; Formal Analysis: KM, VB, AFAJ, CR; Data curation: KM, CR, DWTG, DF, IM, MKS, MKD, MDM, NMD, POW, RS, RK, TYG, VAV, WW; Validation: KM, CR; Visualization: KM, CR; Supervision: AFAJ; Writing- original draft preparation: KM, AFAJ; Writing- review & editing: BG, WT, CR, MAM, JM, YG, MKS, VAV, and AFAJ.

Competing Interests

No authors have any competing interests.

References

Agudelo-Vera, Claudia M., Wouter R. W. A. Leduc, Adriaan R. Mels, and Huub H. M. Rijnaarts. "Harvesting Urban Resources towards More Resilient Cities." *Resources, Conservation and Recycling*, Climate Proofing Cities, 64 (July 1, 2012): 3–12. https://doi.org/10.1016/j.resconrec.2012.01.014.

Ammoura, L., Xueref-Remy, I., Gros, V., Baudic, A., Bonsang, B., Petit, J.-E., Perrussel, O., Bonnaire, N., Sciare, J., and Chevallier, F.: Atmospheric measurements of ratios between CO2 and co-emitted species from traffic: A tunnel study in the Paris megacity, Atmos. Chem. Phys., 14, 12871–12882, https://doi.org/10.5194/acp-14-12871-2014, 2014.

Andela, N., Morton, D. C., Giglio, L., Chen, Y., van der Werf, G. R., Kasibhatla, P. S., DeFries, R. S., Collatz, G. J., Hantson, S., Kloster, S., Bachelet, D., Forrest, M., Lasslop, G., Li, F., Mangeon, S., Melton, J. R., Yue, C., and Randerson, J. T.: A human-driven decline in global burned area, Science, 356, 1356–1362, https://doi.org/10.1126/science.aal4108, 2017.

Anderson, D. C., Loughner, C. P., Diskin, G., Weinheimer, A., Canty, T. P., Salawitch, R. J., Worden, H. M., et al.: Measured and modeled CO and NOy in DISCOVER-AQ: An evaluation of emissions and chemistry over the eastern US, Atmos. Environ., 96, 78–87, https://doi.org/10.1016/j.atmosenv.2014.07.004, 2014.

Andreae, M. O., Andreae, T. W., Annegarn, H., Beer, J., Cachier, H., Le Canut, P., Elbert, W., et al.: Airborne studies of aerosol emissions from savanna fires in southern Africa: 2. Aerosol chemical composition, J. Geophys. Res.: Atmos., 103, 32119–32128, https://doi.org/10.1029/98JD02280, 1998.

Andreae, M. O., Browell, E. V., Garstang, M., Gregory, G. L., Harriss, R. C., Hill, G. F., Jacob, D. J., et al.: Biomass-burning emissions and associated haze layers over Amazonia, J. Geophys. Res.: Atmos., 93, 1509–1527, https://doi.org/10.1029/JD093iD02p01509, 1988.

Andreae, M. O., and Merlet, P.: Emission of trace gases and aerosols from biomass burning, Global Biogeochem. Cycles, 15, 955–966, https://doi.org/10.1029/2000GB001382, 2001.

Andreae, M. O.: Emission of trace gases and aerosols from biomass burning – an updated assessment, Atmos. Chem. Phys., 19, 8523–8546, https://doi.org/10.5194/acp-19-8523-2019, 2019.

Arioli, M. S., D'Agosto, M. A., Amaral, F. G., and Cybis, H. B. B.: The evolution of city-scale GHG emissions inventory methods: A systematic review, Environ. Impact Assess. Rev., 80, 106316, https://doi.org/10.1016/j.eiar.2019.106316, 2020.

Arneth, A., Sitch, S., Pongratz, J., Stocker, B. D., Ciais, P., Poulter, B., Bayer, A. D., et al.: Historical carbon dioxide emissions caused by land-use changes are possibly larger than assumed, Nat. Geosci., 10, 79–84, https://doi.org/10.1038/ngeo2882, 2017.

Bai, X., Dawson, R. J., Ürge-Vorsatz, D., Delgado, G. C., Barau, A. S., Dhakal, S., Dodman, D., et al.: Six research priorities for cities and climate change, Nature, 555, 23–25, https://doi.org/10.1038/d41586-018-02409-z, 2018.

Baiocchi, G., Creutzig, F., Minx, J., and Pichler, P.-P.: A spatial typology of human settlements and their CO2 emissions in England, Glob. Environ. Change, 34, 13–21, https://doi.org/10.1016/j.gloenvcha.2015.06.001, 2015.

Bakwin, P. S., Tans, P. P., Zhao, C., Ussler, W. III, and Quesnell, E.: Measurements of carbon dioxide on a very tall tower, Tellus B, 47, 535–549, https://doi.org/10.1034/j.1600-0889.47.issue5.2.x, 1995.

Banerjee, R., Inamdar, A. B., Phulluke, S., and Pateriya, B.: Decision support system for energy planning in a district: Residential module, Econ. Polit. Wkly., 34, 3545–3552, 1999.

Bares, R., Lin, J. C., Hoch, S. W., Baasandorj, M., Mendoza, D. L., Fasoli, B., Mitchell, L., Catharine, D., and Stephens, B. B.: The wintertime covariation of CO2 and criteria pollutants in an urban valley of the western United States, J. Geophys. Res. Atmos., 123, 2684–2703, https://doi.org/10.1002/2017JD027917, 2018.

Bartholomew, G. W., and Alexander, M.: Soil as a sink for atmospheric carbon monoxide, Science, 212, 1389–1391, https://doi.org/10.1126/science.212.4501.1389, 1981.

Bettencourt, L. M. A., Lobo, J., Helbing, D., Kühnert, C., and West, G. B.: Growth, innovation, scaling, and the pace of life in cities, Proc. Natl. Acad. Sci. USA, 104, 7301–7306, https://doi.org/10.1073/pnas.0610172104, 2007.

Borsdorff, T., aan de Brugh, J., Hu, H., Hasekamp, O., Sussmann, R., Rettinger, M., Hase, F., et al.: Mapping carbon monoxide pollution from space down to city scales with daily global coverage, Atmos. Meas. Tech., 11, 5507–5518, https://doi.org/10.5194/amt-11-5507-2018, 2018.

Bozhinova, D., van der Molen, M. K., van der Velde, I. R., Krol, M. C., van der Laan, S., Meijer, H. A. J., and Peters, W.: Simulating the integrated summertime Δ14CO2 signature from anthropogenic emissions over Western Europe, Atmos. Chem. Phys., 14, 7273–7290, https://doi.org/10.5194/acp-14-7273-2014, 2014.

Bremer, H., Kar, J., Drummond, J. R., Nichitu, F., Zou, J., Liu, J., Gille, J. C., et al.: Carbon monoxide from biomass burning in the tropics and its impact on the tropospheric ozone, J. Geophys. Res. Atmos., 109, D12304, 2004.

Briggs, N. L., Jaffe, D. A., Gao, H., Hee, J. R., Baylon, P. M., Zhang, Q., Zhou, S., Collier, S. C., Sampson, P. D., and Cary, R. A.: Particulate matter, ozone, and nitrogen species in aged wildfire plumes observed at the Mount Bachelor Observatory, Aerosol Air Qual. Res., 16, 3075–3087, https://doi.org/10.4209/aaqr.2016.03.0120, 2016.

Buchholz, R. R., Paton-Walsh, C., Griffith, D. W. T., Kubistin, D., Caldow, C., Fisher, J. A., Deutscher, N. M., et al.: Source and meteorological influences on air quality (CO, CH4 & CO2) at a southern hemisphere urban site, Atmos. Environ., 126, 274–289, https://doi.org/10.1016/j.atmosenv.2015.11.041, 2016.

Buchholz, R. R., Worden, H. M., Park, M., Francis, G., Deeter, M. N., Edwards, D. P., Emmons, L. K., Gaubert, B., Gille, J., Martínez-Alonso, S., Tang, W., Kumar, R., Drummond, J. R., Clerbaux, C., George, M., Coheur, P.-F., Hurtmans, D., Bowman, K. W., Luo, M., Payne, V. H., Worden, J. R., Chin, M., Levy, R. C., Warner, J., Wei, Z., and Kulawik, S. S.: Air pollution trends measured from Terra: CO and AOD over industrial, fire-prone, and background regions, Remote Sens. Environ, 256, 112275, https://doi.org/10.1016/j.rse.2020.112275, 2021.

Bukosa, B., Deutscher, N. M., Fisher, J. A., Kubistin, D., Paton-Walsh, C., and Griffith, D. W. T.: Simultaneous shipborne measurements of CO_2, CH_4 and CO and their application to improving greenhouse-gas flux estimates in Australia, Atmos. Chem. Phys., 19, 7055–7072, https://doi.org/10.5194/acp-19-7055-2019, 2019.

Chandra, N., Patra, P. K., Bisht, J. S. H., Ito, A., Umezawa, T., Saigusa, N., Morimoto, S., et al.: Emissions from the oil and gas sectors, coal mining and ruminant farming drive methane growth over the past three decades, J. Meteorol. Soc. Jpn. Ser. II, 99, 309–337, https://doi.org/10.2151/jmsj.2021-015, 2021.

Chatfield, R. B., Andreae, M. O., ARCTAS Science Team, and SEAC4RS Science Team: Emissions relationships in western forest fire plumes – part 1: Reducing the effect of mixing errors on emission factors, Atmos. Meas. Tech., 13, 7069–7096, https://doi.org/10.5194/amt-13-7069-2020, 2020.

Cheng, Y., Wang, Y., Zhang, Y., Chen, G., Crawford, J. H., Kleb, M. M., Diskin, G. S., and Weinheimer, A. J.: Large biogenic contribution to boundary layer O3-CO regression slope in summer, Geophys. Res. Lett., 44, 7061–7068, https://doi.org/10.1002/2017GL074405, 2017.

Chevallier, F., Remaud, M., O'Dell, C. W., Baker, D., Peylin, P., and Cozic, A.: Objective evaluation of surface- and satellite-driven carbon dioxide atmospheric inversions, Atmos. Chem. Phys., 19, 14233–14251, https://doi.org/10.5194/acp-19-14233-2019, 2019.

Ciais, P., Tan, J., Wang, X., Roedenbeck, C., Chevallier, F., Piao, S.-L., Moriarty, R., Broquet, G., Le Quéré, C., Canadell, J. G., Peng, S., Poulter, B., Liu, Z., and Tans, P.: Five decades of northern land carbon uptake revealed by the interhemispheric CO2 gradient, Nature, 568, 221–225, https://doi.org/10.1038/s41586-019-1078-6, 2019.

Cordero, P. R. F., Bayly, K., Leung, P. M., Huang, C., Islam, Z. F., Schittenhelm, R. B., King, G. M., and Greening, C.: Atmospheric carbon monoxide oxidation is a widespread mechanism supporting microbial survival, ISME J., 13, 2868–2881, https://doi.org/10.1038/s41396-019-0479-8, 2019.

Creutzig, F., Baiocchi, G., Bierkandt, R., Pichler, P.-P., and Seto, K. C.: Global typology of urban energy use and potentials for an urbanization mitigation wedge, Proc. Natl. Acad. Sci. USA, 112, 6283–6288, https://doi.org/10.1073/pnas.1315545112, 2015.

Creutzig, F., Lohrey, S., Bai, X., Baklanov, A., Dawson, R., Dhakal, S., Lamb, W. F., et al.: Upscaling urban data science for global climate solutions, Global Sustain., 2, e2, https://doi.org/10.1017/sus.2018.16, 2019.

Crowell, S., Baker, D., Schuh, A., Basu, S., Jacobson, A. R., Chevallier, F., Liu, J., et al.: The 2015–2016 carbon cycle as seen from OCO-2 and the global in situ network, Atmos. Chem. Phys., 19, 9797–9831, https://doi.org/10.5194/acp-19-9797-2019, 2019.

De Mazière, M., Sha, M. K., Desmet, F., Hermans, C., Scolas, F., Kumps, N., Metzger, J. M., Duflot, V., and Cammas, J. P.: TCCON data from Réunion Island (RE), release GGG2014. R0, TCCON Data Archive, hosted by CaltechDATA, 2017.

Deutscher, N. M., Griffith, D. W. T., Bryant, G. W., Wennberg, P. O., Toon, G. C., Washenfelder, R. A., Keppel-Aleks, G., Wunch, D., Yavin, Y. G., Allen, N. T., Blavier, J.-F. L., Jimenez, R., Daube, B. C., Bright, A. V., Matross, D. M., Wofsy, S. C., and Park, S.: Total column CO2 measurements at Darwin, Australia – site description and calibration against in situ aircraft profiles, Atmos. Meas. Tech., 3, 947–958, https://doi.org/10.5194/amt-3-947-2010, 2010.

Djuricin, S., Pataki, D. E., and Xu, X.: A comparison of tracer methods for quantifying CO2 sources in an urban region, J. Geophys. Res.-Atmos., 115, D11, https://doi.org/10.1029/2009JD012236, 2010.

Dodman, D.: Blaming cities for climate change? An analysis of urban greenhouse gas emissions inventories, Environ. Urban., 21, 185–201, https://doi.org/10.1177/0956247809103016, 2009.

Dowdy, A. J.: Climatological Variability of Fire Weather in Australia, Journalhttps://doi.org/10.1175/JAMC-D-17-0167.1, 2018.

Dubey, M. K., Henderson, B. G., Green, D., Butterfield, Z. T., Keppel-Aleks, G., Allen, N. T., Blavier, J.-F., Roehl, C. M., Wunch, D., and Lindenmaier, R.: TCCON data from Manaus (BR), release GGG2014.R0, CaltechDATA, https://doi.org/10.14291/TCCON.GGG2014.MANAUS01.R0/1149274, 2014.

Edwards, E.-L., Reid, J. S., Xian, P., Burton, S. P., Cook, A. L., Crosbie, E. C., Fenn, M. A., Ferrare, R. A., Freeman, S. W., Hair, J. W., Harper, D. B., Hostetler, C. A., Robinson, C. E., Scarino, A. J., Shook, M. A., Sokolowsky, G. A., van den Heever, S. C., Winstead, E. L., Woods, S., Ziemba, L. D., and Sorooshian, A.: Assessment of NAAPS-RA performance in Maritime Southeast Asia during CAMP^{2}Ex, Atmospheric Chemistry and Physics, 22, 12961–12983, https://doi.org/10.5194/acp-22-12961-2022, 2022.

Erickson, P. and Morgenstern, T.: Fixing greenhouse gas accounting at the city scale, Carbon Manag, 7, 313–316, https://doi.org/10.1080/17583004.2016.1238743, 2016.

Feist, D., Arnold, S., John, N., and Geibel, M.: TCCON data from ascension island (SH), release GGG2014. R0, TCCON data archive, hosted by CaltechDATA, 2014.

Fisher, J. A., Wilson, S. R., Zeng, G., Williams, J. E., Emmons, L. K., Langenfelds, R. L., Krummel, P. B., and Steele, L. P.: Seasonal changes in the tropospheric carbon monoxide profile over the remote Southern Hemisphere evaluated using multi-model simulations and aircraft observations, Atmos. Chem. Phys., 15, 3217–3239, https://doi.org/10.5194/acp-15-3217-2015, 2015.

Frankenberg, C., Pollock, R., Lee, R. A. M., Rosenberg, R., Blavier, J.-F., Crisp, D., O'Dell, C. W., et al.: The Orbiting Carbon Observatory (OCO-2): Spectrometer Performance Evaluation Using Pre-Launch Direct Sun Measurements, Atmos. Meas. Tech., 8, 301–313, https://doi.org/10.5194/amt-8-301-2015, 2015.

Friedlingstein, P., Jones, M. W., O'Sullivan, M., Andrew, R. M., Bakker, D. C. E., Hauck, J., Le Quéré, C., et al.: Global Carbon Budget 2021, Earth Syst. Sci. Data, 14, 1917–2005, https://doi.org/10.5194/essd-14-1917-2022, 2022.

Gately, C. K., and Hutyra, L. R.: Large Uncertainties in Urban-Scale Carbon Emissions, J. Geophys. Res. Atmos., 122, 11242–11260, https://doi.org/10.1002/2017JD027359, 2017.

Gaubert, B., Arellano, A. F. Jr., Barré, J., Worden, H. M., Emmons, L. K., Tilmes, S., Buchholz, R. R., et al.: Toward a Chemical Reanalysis in a Coupled Chemistry-Climate Model: An Evaluation of MOPITT CO Assimilation and Its Impact on Tropospheric Composition, J. Geophys. Res. Atmos., 121, 7310–7343, https://doi.org/10.1002/2016JD024863, 2016.

Gaubert, B., Worden, H. M., Arellano, A. F. J., Emmons, L. K., Tilmes, S., Barré, J., Martinez Alonso, S., et al.: Chemical Feedback From Decreasing Carbon Monoxide Emissions, Geophys. Res. Lett., 44, 9985–9995, https://doi.org/10.1002/2017GL074987, 2017.

Gaubert, B., Stephens, B. B., Basu, S., Chevallier, F., Deng, F., Kort, E. A., Patra, P. K., et al.: Global Atmospheric CO2 Inverse Models Converging on Neutral Tropical Land Exchange, but Disagreeing on Fossil Fuel and Atmospheric Growth Rate, Biogeosciences, 16, 117–134, https://doi.org/10.5194/bg-16-117-2019, 2019.

Geibel, M. C., Gerbig, C., and Feist, D. G.: A New Fully Automated FTIR System for Total Column Measurements of Greenhouse Gases, Atmos. Meas. Tech., 3, 1363–1375, https://doi.org/10.5194/amt-3-1363-2010, 2010.

Giglio, L., Randerson, J. T., and van der Werf, G. R.: Analysis of Daily, Monthly, and Annual Burned Area Using the Fourth-Generation Global Fire Emissions Database (GFED4), J. Geophys. Res. Biogeosci., 118, 317–328, https://doi.org/10.1002/jgrg.20042, 2013.

Goo, T.-Y., Oh, Y.-S., and Velazco, V. A.: TCCON Data from Anmeyondo (KR), Release GGG2014.R0, CaltechDATA, https://doi.org/10.14291/TCCON.GGG2014.ANMEYONDO01.R0/1149284, 2014.

Granier, C., Darras, S., Denier van der Gon, H., Doubalova, J., Elguindi, N., Galle, B., Gauss, M., et al.: The Copernicus Atmosphere Monitoring Service Global and Regional Emissions (April 2019 Version), https://doi.org/10.24380/D0BN-KX16, 2019.

Griffith, D. W. T., Deutscher, N. M., Velazco, V. A., Wennberg, P. O., Yavin, Y., Keppel-Aleks, G., Washenfelder, R. A., et al.: TCCON Data from Darwin (AU), Release GGG2014.R0, CaltechDATA, https://doi.org/10.14291/TCCON.GGG2014.DARWIN01.R0/1149290, 2014.

Griffith, D. W. T., Velazco, V. A., Deutscher, N. M., Paton-Walsh, C., Jones, N. B., Wilson, S. R., Macatangay, R. C., Kettlewell, G. C., Buchholz, R. R., and Riggenbach, M. O.: TCCON Data from Wollongong (AU), Release GGG2014.R0, CaltechDATA, https://doi.org/10.14291/TCCON.GGG2014.WOLLONGONG01.R0/1149291, 2014.

Grimm, N. B., Faeth, S. H., Golubiewski, N. E., Redman, C. L., Wu, J., Bai, X., and Briggs, J. M.: Global Change and the Ecology of Cities, Science, 319, 756–760, https://doi.org/10.1126/science.1150195, 2008.

Gurney, K. R., Chen, Y.-H., Maki, T., Kawa, S. R., Andrews, A., and Zhu, Z.: Sensitivity of Atmospheric CO2 Inversions to Seasonal and Interannual Variations in Fossil Fuel Emissions, J. Geophys. Res. Atmos., 110, D10, https://doi.org/10.1029/2004JD005373, 2005.

Gurney, K. R., Song, Y., Liang, J., and Roest, G.: Toward Accurate, Policy-Relevant Fossil Fuel CO2 Emission Landscapes, Environ. Sci. Technol., 54, 9896–9907, https://doi.org/10.1021/acs.est.0c01175, 2020.

Guthrie, P. D.: The CH4 - CO - OH Conundrum: A Simple Analytic Approach, Global Biogeochem. Cycles, 3, 287–298, https://doi.org/10.1029/GB003i004p00287, 1989.

Guyon, P., Frank, G. P., Welling, M., Chand, D., Artaxo, P., Rizzo, L., Nishioka, G., et al.: Airborne Measurements of Trace Gas and Aerosol Particle Emissions from Biomass Burning in Amazonia, Atmos. Chem. Phys., 5, 2989–3002, https://doi.org/10.5194/acp-5-2989-2005, 2005.

Halliday, H. S., DiGangi, J. P., Choi, Y., Diskin, G. S., Pusede, S. E., Rana, M., Nowak, J. B., et al.: Using Short-Term CO/CO2 Ratios to Assess Air Mass Differences Over the Korean Peninsula During KORUS-AQ, J. Geophys. Res. Atmos., 124, 10951–10972, https://doi.org/10.1029/2018JD029697, 2019.

Hedelius, J. K., Liu, J., Oda, T., Maksyutov, S., Roehl, C. M., Iraci, L. T., Podolske, J. R., et al.: Southern California Megacity CO2, CH4, and CO Flux Estimates Using Ground- and Space-Based Remote Sensing and a Lagrangian Model, Atmos. Chem. Phys., 18, 16271–16291, https://doi.org/10.5194/acp-18-16271-2018, 2018.

Hickman, J. E., Andela, N., Tsigaridis, K., Galy-Lacaux, C., Ossohou, M., and Bauer, S. E.: Reductions in NO2 Burden over North Equatorial Africa from Decline in Biomass Burning in Spite of Growing Fossil Fuel Use, 2005 to 2017, Proc. Natl. Acad. Sci. U.S.A., 118, e2002579118, https://doi.org/10.1073/pnas.2002579118, 2021.

Hilario, M. R. A., Crosbie, E., Shook, M., Reid, J. S., Cambaliza, M. O. L., Simpas, J. B. B., and Sorooshian, A.: Measurement report: Long-range transport patterns into the tropical northwest Pacific during the CAMP2Ex aircraft campaign: chemical composition, size distributions, and the impact of convection, Atmos. Chem. Phys., 21, 3777–3802, 2021.

Hobbs, P. V., Sinha, P., Yokelson, R. J., Christian, T. J., Blake, D. R., Gao, S., Kirchstetter, T. W., Novakov, T., and Pilewskie, P.: Evolution of Gases and Particles from a Savanna Fire in South Africa, J. Geophys. Res. Atmos., 108, D13, https://doi.org/10.1029/2002JD002352, 2003.

Hoesly, R. M., Smith, S. J., Feng, L., Klimont, Z., Janssens-Maenhout, G., Pitkanen, T., Seibert, J. J., et al.: Historical (1750–2014) Anthropogenic Emissions of Reactive Gases and Aerosols from the Community Emissions Data System (CEDS), Geosci. Model Dev., 11, 369–408, https://doi.org/10.5194/gmd-11-369-2018, 2018.

Houweling, S., Baker, D., Basu, S., Boesch, H., Butz, A., Chevallier, F., Deng, F., et al.: An Intercomparison of Inverse Models for Estimating Sources and Sinks of CO2 Using GOSAT Measurements, J. Geophys. Res. Atmos., 120, 5253–5266, https://doi.org/10.1002/2014JD022962, 2015.

Houweling, S., Bergamaschi, P., Chevallier, F., Heimann, M., Kaminski, T., Krol, M., Michalak, A. M., and Patra, P.: Global Inverse Modeling of CH_4 Sources and Sinks: An Overview of Methods, Atmos. Chem. Phys., 17, 235–256, https://doi.org/10.5194/acp-17-235-2017, 2017.

Hutyra, L. R., Duren, R., Gurney, K. R., Grimm, N., Kort, E. A., Larson, E., and Shrestha, G.: Urbanization and the Carbon Cycle: Current Capabilities and Research Outlook from the Natural Sciences Perspective, Earth's Future, 2, 473–495, https://doi.org/10.1002/2014EF000255, 2014.

Kennedy, C., Steinberger, J., Gasson, B., Hansen, Y., Hillman, T., Havránek, M., Pataki, D., Phdungsilp, A., Ramaswami, A., and Villalba Mendez, G.: Greenhouse Gas Emissions from Global Cities, Environ. Sci. Technol., 43, 7297–7302, https://doi.org/10.1021/es900213p, 2009.

Kennedy, C. A., Stewart, I., Facchini, A., Cersosimo, I., Mele, R., Chen, B., Uda, M., et al.: Energy and Material Flows of Megacities, Proc. Natl. Acad. Sci. U.S.A., 112, 5985–5990, https://doi.org/10.1073/pnas.1504315112, 2015.

Khalil, M. A. K., and Rasmussen, R. A.: The Global Cycle of Carbon Monoxide: Trends and Mass Balance, Chemosphere, 20, 227–242, https://doi.org/10.1016/0045-6535(90)90098-E, 1990.

Kivi, R., Heikkinen, P., Kyro, E., "TCCON Data from Sodankyla, Finland, Release GGG2014R0," TCCON Data Archive, Hosted by CaltechDATA, California Institute of Technology, Pasadena, CA, U.S.A., https://doi.org/10.14291/tccon.ggg2014.sodankyla01.R0/1149280, 2014.

Kong, Y., Chen, B., and Measho, S.: Spatio-Temporal Consistency Evaluation of XCO2 Retrievals from GOSAT and OCO-2 Based on TCCON and Model Data for Joint Utilization in Carbon Cycle Research, Atmosphere, 10, 354, https://doi.org/10.3390/atmos10070354, 2019.

Kraskov, A., Stögbauer, H., and Grassberger, P.: Estimating Mutual Information, Phys. Rev. E, 69, 066138, https://doi.org/10.1103/PhysRevE.69.066138, 2004.

Kulawik, S., Wunch, D., O'Dell, C., Frankenberg, C., Reuter, M., Oda, T., Chevallier, F., et al.: Consistent Evaluation of ACOS-GOSAT, BESD-SCIAMACHY, CarbonTracker, and MACC through Comparisons to TCCON, Atmos. Meas. Tech., 9, 683–709, https://doi.org/10.5194/amt-9-683-2016, 2016.

Kumar, A., Mishra, S., Bakshi, S., Upadhyay, P., and Thakur, T. K.: Response of Eutrophication and Water Quality Drivers on Greenhouse Gas Emissions in Lakes of China: A Critical Analysis, Ecohydrology, 16, e2483, https://doi.org/10.1002/eco.2483, 2023.

Lamb, W. F., Wiedmann, T., Pongratz, J., Andrew, R., Crippa, M., Olivier, J. G. J., Wiedenhofer, D., et al.: A Review of Trends and Drivers of Greenhouse Gas Emissions by Sector from 1990 to 2018, Environ. Res. Lett., 16, 073005, https://doi.org/10.1088/1748-9326/abee4e, 2021.

Le Canut, P., Andreae, M. O., Harris, G. W., Wienhold, F. G., and Zenker, T.: Airborne Studies of Emissions from Savanna Fires in Southern Africa: 1. Aerosol Emissions Measured with a Laser Optical Particle Counter, J. Geophys. Res., 101, 23615–23630, https://doi.org/10.1029/95JD02610, 1996.

Lee, H., Dlugokencky, E. J., Turnbull, J. C., Lee, S., Lehman, S. J., Miller, J. B., Pétron, G., et al.: Observations of Atmospheric 14CO2 at Anmyeondo GAW Station, South Korea: Implications for Fossil Fuel CO2 and Emission Ratios, Atmos. Chem. Phys., 20, 12033–12045, https://doi.org/10.5194/acp-20-12033-2020, 2020.

Lefer, B. L., Talbot, R. W., Harriss, R. H., Bradshaw, J. D., Sandholm, S. T., Olson, J. O., Sachse, G. W., et al.: Enhancement of Acidic Gases in Biomass Burning Impacted Air Masses over Canada, J. Geophys. Res., 99, 1721–1737, https://doi.org/10.1029/93JD02091, 1994.

Lelieveld, J., Peters, W., Dentener, F. J., and Krol, M. C.: Stability of Tropospheric Hydroxyl Chemistry, J. Geophys. Res., 107, ACH 17-1-ACH 17-11, https://doi.org/10.1029/2002JD002272, 2002.

Lelieveld, J., Gromov, S., Pozzer, A., and Taraborrelli, D.: Global tropospheric hydroxyl distribution, budget and reactivity, Atmos. Chem. Phys., 16, 12477–12493, https://doi.org/10.5194/acp-16-12477-2016, 2016.

Levin, I., Kromer, B., Schmidt, M., and Sartorius, H.: A Novel Approach for Independent Budgeting of Fossil Fuel CO2 over Europe by 14CO2 Observations, Geophys. Res. Lett., 30, https://doi.org/10.1029/2003GL018477, 2003.

Levy, H.: Normal Atmosphere: Large Radical and Formaldehyde Concentrations Predicted, Science, 173, 141–143, https://doi.org/10.1126/science.173.3992.141, 1971.

Liang, A., Gong, W., Han, G., and Xiang, C.: Comparison of Satellite-Observed XCO2 from GOSAT, OCO-2, and Ground-Based TCCON, Remote Sens., 9, 1033, https://doi.org/10.3390/rs9101033, 2017.

Liu, C., Wang, W., and Sun, Y.: TCCON Data from Hefei (PRC), Release GGG2014.R0, Application/x-netcdf, CaltechDATA, https://doi.org/10.14291/TCCON.GGG2014.HEFEI01.R0, 2018.

Lu, X., Jacob, D. J., Zhang, Y., Maasakkers, J. D., Sulprizio, M. P., Shen, L., Qu, Z., et al.: Global Methane Budget and Trend, 2010–2017: Complementarity of Inverse Analyses Using in Situ (GLOBALVIEWplus CH4 ObsPack) and Satellite (GOSAT) Observations, Atmos. Chem. Phys., 21, 4637–4657, https://doi.org/10.5194/acp-21-4637-2021, 2021.

Lunt, M. F., Palmer, P. I., Feng, L., Taylor, C. M., Boesch, H., and Parker, R. J.: An Increase in Methane Emissions from Tropical Africa between 2010 and 2016 Inferred from Satellite Data, Atmos. Chem. Phys., 19, 14721–14740, https://doi.org/10.5194/acp-19-14721-2019, 2019.

Maasakkers, J. D., Jacob, D. J., Sulprizio, M. P., Scarpelli, T. R., Nesser, H., Sheng, J.-X., Zhang, Y., et al.: Global Distribution of Methane Emissions, Emission Trends, and OH Concentrations and Trends Inferred from an Inversion of GOSAT Satellite Data for 2010–2015, Atmos. Chem. Phys., 19, 7859–7881, https://doi.org/10.5194/acp-19-7859-2019, 2019.

Mauzerall, D. L., Logan, J. A., Jacob, D. J., Anderson, B. E., Blake, D. R., Bradshaw, J. D., Heikes, B., Sachse, G. W., Singh, H., and Talbot, B.: Photochemistry in Biomass Burning Plumes and Implications for Tropospheric Ozone over the Tropical South Atlantic, J. Geophys. Res., 103, 8401–8423, https://doi.org/10.1029/97JD02612, 1998.

Miller, C. E., Crisp, D., DeCola, P. L., Olsen, S. C., Randerson, J. T., Michalak, A. M., Alkhaled, A., et al.: Precision Requirements for Space-Based Data, J. Geophys. Res., 112, D10314, https://doi.org/10.1029/2006JD007659, 2007.

Moore, B. III, Crowell, S. M. R., Rayner, P. J., Kumer, J., O'Dell, C. W., O'Brien, D., Utembe, S., Polonsky, I., Schimel, D., and Lemen, J.: The Potential of the Geostationary Carbon Cycle Observatory (GeoCarb) to Provide Multi-Scale Constraints on the Carbon Cycle in the Americas, Front. Environ. Sci., 6, 109, https://www.frontiersin.org/articles/10.3389/fenvs.2018.00109, 2018.

Morino, I., Uchino, O., Inoue, M., Yoshida, Y., Yokota, T., Wennberg, P. O., Toon, G. C., et al.: Preliminary Validation of Column-Averaged Volume Mixing Ratios of Carbon Dioxide and Methane Retrieved from GOSAT Short-Wavelength Infrared Spectra, Atmos. Meas. Tech., 4, 1061–1076, https://doi.org/10.5194/amt-4-1061-2011, 2011.

Nassar, R., Napier-Linton, L., Gurney, K. R., Andres, R. J., Oda, T., Vogel, F. R., and Deng, F.: Improving the Temporal and Spatial Distribution of CO2 Emissions from Global Fossil Fuel Emission Data Sets, J. Geophys. Res., 118, 917–933, https://doi.org/10.1029/2012JD018196, 2013.

Oda, T., Bun, R., Kinakh, V., Topylko, P., Halushchak, M., Marland, G., Lauvaux, T., et al.: Errors and Uncertainties in a Gridded Carbon Dioxide Emissions Inventory, Mitig. Adapt. Strateg. Glob. Change, 24, 1007–1050, https://doi.org/10.1007/s11027-019-09877-2, 2019.

Oh, Y.-S., Kenea, S. T., Goo, T.-Y., Chung, K.-S., Rhee, J.-S., Ou, M.-L., Byun, Y.-H., et al.: Characteristics of Greenhouse Gas Concentrations Derived from Ground-Based FTS Spectra at Anmyeondo, South Korea, Atmos. Meas. Tech., 11, 2361–2374, https://doi.org/10.5194/amt-11-2361-2018, 2018.

Palmer, P. I., Suntharalingam, P., Jones, D. B. A., Jacob, D. J., Streets, D. G., Fu, Q., Vay, S. A., et al.: Using CO2 Correlations to Improve Inverse Analyses of Carbon Fluxes, J. Geophys. Res., 111, D12318, https://doi.org/10.1029/2005JD006697, 2006.

Palmer, P. I., Feng, L., Baker, D., Chevallier, F., Bösch, H., and Somkuti, P.: Net Carbon Emissions from African Biosphere Dominate Pan-Tropical Atmospheric CO2 Signal, Nat. Commun., 10, 3344, https://doi.org/10.1038/s41467-019-11097-w, 2019.

Parker, R. J., Boesch, H., Wooster, M. J., Moore, D. P., Webb, A. J., Gaveau, D., and Murdiyarso, D.: Atmospheric CH4 and CO2 Enhancements and Biomass Burning Emission Ratios Derived from Satellite Observations of the 2015 Indonesian Fire Plumes, Atmos. Chem. Phys., 16, 10111–10131, https://doi.org/10.5194/acp-16-10111-2016, 2016.

Peylin, P., Houweling, S., Krol, M. C., Karstens, U., Rödenbeck, C., Geels, C., Vermeulen, A., et al.: Importance of Fossil Fuel Emission Uncertainties over Europe for CO_2 Modeling: Model Intercomparison, Atmos. Chem. Phys., 11, 6607–6622, https://doi.org/10.5194/acp-11-6607-2011, 2011.

Peylin, P., Law, R. M., Gurney, K. R., Chevallier, F., Jacobson, A. R., Maki, T., Niwa, Y., et al.: Global Atmospheric Carbon Budget: Results from an Ensemble of Atmospheric CO_2 Inversions, Biogeosciences, 10, 6699–6720, https://doi.org/10.5194/bg-10-6699-2013, 2013.

Plant, G., Kort, E. A., Murray, L. T., Maasakkers, J. D., and Aben, I.: Evaluating Urban Methane Emissions from Space Using TROPOMI Methane and Carbon Monoxide Observations, Remote Sens. Environ., 268, 112756, https://doi.org/10.1016/j.rse.2021.112756, 2022.

Popa, M. E., Vollmer, M. K., Jordan, A., Brand, W. A., Pathirana, S. L., Rothe, M., and Röckmann, T.: Vehicle Emissions of Greenhouse Gases and Related Tracers from a Tunnel Study: CO : CO_2, N_2O : CO_2, CH_4 : CO_2, O_2 : CO_2 Ratios, and the Stable Isotopes ^{13}C and ^{18}O in CO_2 and CO. Atmos. Chem. Phys., 14, 2105–2123, https://doi.org/10.5194/acp-14-2105-2014, 2014.

Prather, M. J.: Lifetimes and Eigenstates in Atmospheric Chemistry, Geophys. Res. Lett., 21, 801–804, https://doi.org/10.1029/94GL00840, 1994.

Qu, Z., Jacob, D. J., Shen, L., Lu, X., Zhang, Y., Scarpelli, T. R., Nesser, H., et al.: Global Distribution of Methane Emissions: A Comparative Inverse Analysis of Observations from the TROPOMI and GOSAT Satellite Instruments, Atmos. Chem. Phys., 21, 14159–14175, https://doi.org/10.5194/acp-21-14159-2021, 2021.

Röckmann, T., Gómez Álvarez, C. X., Walter, S., van der Veen, C., Wollny, A. G., Gunthe, S. S., Helas, G., et al.: Isotopic Composition of H_2 from Wood Burning: Dependency on Combustion Efficiency, Moisture Content, and ΔD of Local Precipitation, J. Geophys. Res., 115, D17308, https://doi.org/10.1029/2009JD013188, 2010.

Saeki, T., and Patra, P. K.: Implications of Overestimated Anthropogenic CO2 Emissions on East Asian and Global Land CO2 Flux Inversion, Geosci. Lett., 4, 9, https://doi.org/10.1186/s40562-017-0074-7, 2017.

Saunois, M., Stavert, A. R., Poulter, B., Bousquet, P., Canadell, J. G., Jackson, R. B., Raymond, P. A., et al.: The Global Methane Budget 2000–2017, Earth Syst. Sci. Data, 12, 1561–1623, https://doi.org/10.5194/essd-12-1561-2020, 2020.

Sha, M. K., Langerock, B., Blavier, J.-F. L., Blumenstock, T., Borsdorff, T., Buschmann, M., Dehn, A., De Mazière, M., Deutscher, N. M., Feist, D. G., García, O. E., Griffith, D. W. T., Grutter, M., Hannigan, J. W., Hase, F., Heikkinen, P., Hermans, C., Iraci, L. T., Jeseck, P., Jones, N., Kivi, R., Kumps, N., Landgraf, J., Lorente, A., Mahieu, E., Makarova, M. V., Mellqvist, J., Metzger, J.-M., Morino, I., Nagahama, T., Notholt, J., Ohyama, H., Ortega, I., Palm, M., Petri, C., Pollard, D. F., Rettinger, M., Robinson, J., Roche, S., Roehl, C. M., Röhling, A. N., Rousogenous, C., Schneider, M., Shiomi, K., Smale, D., Stremme, W., Strong, K., Sussmann, R., Té, Y., Uchino, O., Velazco, V. A., Vigouroux, C., Vrekoussis, M., Wang, P., Warneke, T., Wizenberg, T., Wunch, D., Yamanouchi, S., Yang, Y., and Zhou, M.: Validation of methane and carbon monoxide from Sentinel-5 Precursor using TCCON and NDACC-IRWG stations, Atmos. Meas. Tech., 14, 6249–6304, https://doi.org/10.5194/amt-14-6249-2021, 2021.

Silva, S. J., & Arellano, A. F. (2017). Characterizing regional-scale combustion using satellite retrievals of CO, NO2, and CO2. *Remote Sens.*, *9*(7), 744. https://doi.org/10.3390/rs9070744, 2014.

Silva, S. J., Arellano, A. F., & Worden, H. M.: Toward anthropogenic combustion emission constraints from space-based analysis of urban CO2/CO sensitivity, Geophys. Res. Lett., 40, 4971–4976, https://doi.org/10.1002/grl.50954, 2013.

Sim, S., Lee, H., Oh, E., Kim, S., Ciais, P., Piao, S., Lin, J. C., et al.: Short-term reduction of regional enhancement of atmospheric CO2 in China during the first COVID-19 pandemic period, Environ. Res. Lett., 17, 024036, https://doi.org/10.1088/1748-9326/ac507d, 2022.

Stavert, A. R., Saunois, M., Canadell, J. G., Poulter, B., Jackson, R. B., Regnier, P., Lauerwald, R., et al.: Regional trends and drivers of the global methane budget, Global Change Biol., 28, 182–200, https://doi.org/10.1111/gcb.15901, 2022.

Streets, D. G., Canty, T., Carmichael, G. R., de Foy, B., Dickerson, R. R., Duncan, B. N., Edwards, D. P., et al.: Emissions estimation from satellite retrievals: A review of current capability, Atmos. Environ., 77, 1011–1042, https://doi.org/10.1016/j.atmosenv.2013.05.051, 2013.

Super, I., Denier van der Gon, H. A. C., Visschedijk, A. J. H., Moerman, M. M., Chen, H., van der Molen, M. K., & Peters, W.: Interpreting continuous in-situ observations of carbon dioxide and carbon monoxide in the urban port area of Rotterdam, Atmos. Pollut. Res., 8(1), 174–187, https://doi.org/10.1016/j.apr.2016.08.008, 2017.

Sussmann, R., & Rettinger, M.: TCCON data from Garmisch (DE), Release GGG2014.R2, CaltechDATA, https://doi.org/10.14291/TCCON.GGG2014.GARMISCH01.R2, 2018.

Swap, R., Garstang, M., Macko, S. A., Tyson, P. D., Maenhaut, W., Artaxo, P., Kållberg, P., & Talbot, R.: The long-range transport of Southern African aerosols to the tropical South Atlantic, J. Geophys. Res. Atmos., 101(D19), 23777–23791, https://doi.org/10.1029/95JD01049, 1996.

Sze, N. D.: Anthropogenic CO emissions: Implications for the atmospheric CO-OH-CH4 cycle, Science, 195(4279), 673–675, https://doi.org/10.1126/science.195.4279.673, 1977.

Tang, W., Arellano, A. F., DiGangi, J. P., Choi, Y., Diskin, G. S., Agustí-Panareda, A., Parrington, M., et al.: Evaluating high-resolution forecasts of atmospheric CO and CO2 from a global prediction system during KORUS-AQ field campaign, Atmos. Chem. Phys., 18(15), 11007–11030, https://doi.org/10.5194/acp-18-11007-2018, 2018.

Tang, W., Arellano, A. F., Gaubert, B., Miyazaki, K., & Worden, H. M.: Satellite data reveal a common combustion emission pathway for major cities in China, Atmos. Chem. Phys., 19(7), 4269–4288, https://doi.org/10.5194/acp-19-4269-2019, 2019.

Tang, W., Gaubert, B., Emmons, L., Choi, Y., DiGangi, J. P., Diskin, G. S., Xu, X., et al.: On the relationship between tropospheric CO and CO2 during KORUS-AQ and its role in constraining anthropogenic CO2, Atmos. Chem. Phys. Discuss., https://doi.org/10.5194/acp-2020-864, 2020.

Thompson, R. L., Patra, P. K., Chevallier, F., Maksyutov, S., Law, R. M., Ziehn, T., van der Laan-Luijkx, I. T., et al.: Top–down assessment of the Asian carbon budget since the mid 1990s, Nat. Commun., 7(1), 10724, https://doi.org/10.1038/ncomms10724, 2016.

Tian, Y., Sun, Y., Liu, C., Wang, W., Shan, C., Xu, X., & Hu, Q.: Characterisation of methane variability and trends from near-infrared solar spectra over Hefei, China, Atmos. Environ., 173, 198–209, https://doi.org/10.1016/j.atmosenv.2017.11.001, 2018.

Tilmes, S., Lamarque, J.-F., Emmons, L. K., Kinnison, D. E., Ma, P.-L., Liu, X., Ghan, S., et al.: Description and evaluation of tropospheric chemistry and aerosols in the Community Earth System Model (CESM1.2), Geosci. Model Dev., 8(5), 1395–1426, https://doi.org/10.5194/gmd-8-1395-2015, 2015.

Turnbull, J., Rayner, P., Miller, J., Naegler, T., Ciais, P., & Cozic, A.: On the use of 14CO2 as a tracer for fossil fuel CO2: Quantifying uncertainties using an atmospheric transport model, J. Geophys. Res. Atmos., 114(D22), https://doi.org/10.1029/2009JD012308, 2009.

Turnbull, J. C., Tans, P. P., Lehman, S. J., Baker, D., Conway, T. J., Chung, Y. S., Gregg, J., et al.: Atmospheric observations of carbon monoxide and fossil fuel CO2 emissions from East Asia, J. Geophys. Res. Atmos., 116(D24), https://doi.org/10.1029/2011JD016691, 2011.

Turnbull, J. C., Sweeney, C., Karion, A., Newberger, T., Lehman, S. J., Tans, P. P., Davis, K. J., et al.: Toward quantification and source sector identification of fossil fuel CO2 emissions from an urban area: Results from the INFLUX experiment, J. Geophys. Res. Atmos., 120(1), 292–312, https://doi.org/10.1002/2014JD022555, 2015.

Velazco, V. A., Morino, I., Uchino, O., Hori, A., Kiel, M., Bukosa, B., Deutscher, N. M., et al.: TCCON Philippines: First measurement results, satellite data and model comparisons in Southeast Asia, Remote Sens., 9(12), 1228, https://doi.org/10.3390/rs9121228, 2017.

Verhulst, K. R., Karion, A., Kim, J., Salameh, P. K., Keeling, R. F., Newman, S., Miller, J., et al.: Carbon dioxide and methane measurements from the Los Angeles megacity carbon project – Part 1: Calibration, urban enhancements, and uncertainty estimates, Atmos. Chem. Phys., 17(13), 8313–8341, https://doi.org/10.5194/acp-17-8313-2017, 2017.

Vigouroux, C., Stavrakou, T., Whaley, C., Dils, B., Duflot, V., Hermans, C., Kumps, N., et al.: FTIR time-series of biomass burning products (HCN, C_2H_6, C_2H_2, CH_3OH, and HCOOH) at Reunion Island (21° S, 55° E) and comparisons with model data, Atmos. Chem. Phys., 12(21), 10367–10385, https://doi.org/10.5194/acp-12-10367-2012, 2012.

van Vuuren, D. P., & Riahi, K.: Do recent emission trends imply higher emissions forever? Clim. Change, 91(3), 237–248, https://doi.org/10.1007/s10584-008-9485-y, 2008.

Wang, W., Tian, Y., Liu, C., Sun, Y., Liu, W., Xie, P., Liu, J., et al.: Investigating the performance of a greenhouse gas observatory in Hefei, China, Atmos. Meas. Tech., 10(7), 2627–2643, https://doi.org/10.5194/amt-10-2627-2017, 2017.

Wang, Y., Munger, J. W., Xu, S., McElroy, M. B., Hao, J., Nielsen, C. P., & Ma, H.: CO2 and its correlation with CO at a rural site near Beijing: Implications for combustion efficiency in China, Atmos. Chem. Phys., 10(18), 8881–8897, https://doi.org/10.5194/acp-10-8881-2010, 2010.

Wang, Y., Yuan, Q., Zhou, S., & Zhang, L.: Global spatiotemporal completion of daily high-resolution TCCO from TROPOMI over land using a swath-based local ensemble learning method, ISPRS J. Photogramm. Remote Sens., 194, 167–180, https://doi.org/10.1016/j.isprsjprs.2022.10.012, 2022.

Wei, W., Zhang, W., Hu, D., Ou, L., Tong, Y., Shen, G., Shen, H., & Wang, X.: Emissions of carbon monoxide and carbon dioxide from uncompressed and pelletized biomass fuel burning in typical household stoves in China, Atmos. Environ., 56, 136–142, https://doi.org/10.1016/j.atmosenv.2012.03.060, 2012.

Weisz, H., & Steinberger, J. K.: Reducing energy and material flows in cities, Curr. Opin. Environ. Sustain., 2(3), 185–192, https://doi.org/10.1016/j.cosust.2010.05.010, 2010.

Wennberg, P. O., Wunch, D., Roehl, C. M., Blavier, J.-F., Toon, G. C., & Allen, N. T.: TCCON data from Caltech (US), Release GGG2014.R1, CaltechDATA, June 16, 2015, https://doi.org/10.14291/TCCON.GGG2014.PASADENA01.R1/1182415.

Wennberg, P. O., Mui, W., Wunch, D., Kort, E. A., Blake, D. R., Atlas, E. L., Santoni, G. W., et al.: On the sources of methane to the Los Angeles atmosphere, Environ. Sci. Technol., 46(17), 9282–9289, https://doi.org/10.1021/es301138y, 2012.

Wu, C., & Yu, J. Z.: Evaluation of linear regression techniques for atmospheric applications: the importance of appropriate weighting, Atmos. Meas. Tech., 11, 1233–1250, https://doi.org/10.5194/amt-11-1233-2018, 2018.

Wunch, D., Wennberg, P. O., Toon, G. C., Keppel-Aleks, G., and Yavin, Y. G.: Emissions of greenhouse gases from a North American megacity, Geophys. Res. Lett, 36, https://doi.org/10.1029/2009GL039825, 2009.

Wunch, D., Toon, G. C., Wennberg, P. O., Wofsy, S. C., Stephens, B. B., Fischer, M. L., Uchino, O., et al.: Calibration of the Total Carbon Column Observing Network using aircraft profile data, Atmos. Meas. Tech., 3(5), 1351–1362, https://doi.org/10.5194/amt-3-1351-2010, 2010.

Wunch, D., Wennberg, P. O., Osterman, G., Fisher, B., Naylor, B., Roehl, C. M., O'Dell, C., et al.: Comparisons of the Orbiting Carbon Observatory-2 (OCO-2) XCO_2 measurements with TCCON, Atmos. Meas. Tech., 10(6), 2209–2238, https://doi.org/10.5194/amt-10-2209-2017, 2017.

Wunch, D., Wennberg, P. O., Toon, G. C., Keppel-Aleks, G., & Yavin, Y. G.: Emissions of greenhouse gases from a North American megacity, Geophys. Res. Lett., 36(15), https://doi.org/10.1029/2009GL039825, 2009.

Wunch, D., Toon, G. C., Blavier, J.-F. L., Washenfelder, R. A., Notholt, J., Connor, B. J., Griffith, D. W. T., Sherlock, V., & Wennberg, P. O.: The Total Carbon Column Observing Network, Philos. Trans. R. Soc. A, 369(1943), 2087–2112, https://doi.org/10.1098/rsta.2010.0240, 2011.

Yokelson, R. J., Andreae, M. O., & Akagi, S. K.: Pitfalls with the use of enhancement ratios or normalized excess mixing ratios measured in plumes to characterize pollution sources and aging, Atmos. Meas. Tech., 6(8), 2155–2158, https://doi.org/10.5194/amt-6-2155-2013, 2013.

York, D., Evensen, N. M., López Martínez, M., & De Basabe Delgado, J.: Unified equations for the slope, intercept, and standard errors of the best straight line, Am. J. Phys., 72(3), 367–375, https://doi.org/10.1119/1.1632486, 2004.

Yoshida, Y., Kikuchi, N., Morino, I., Uchino, O., Oshchepkov, S., Bril, A., Saeki, T., et al.: Improvement of the retrieval algorithm for GOSAT SWIR XCO_2 and XCH_4 and their validation using TCCON data, Atmos. Meas. Tech., 6(6), 1533–1547, https://doi.org/10.5194/amt-6-1533-2013, 2013.

Zhang, X., Liu, J., Han, H., Zhang, Y., Jiang, Z., Wang, H., Meng, L., Li, Y. C., & Liu, Y.: Satellite-observed variations and trends in carbon monoxide over Asia and their sensitivities to biomass burning, Remote Sens., 12(5), 830, https://doi.org/10.3390/rs12050830, 2020.

Zhang, Z., Zimmermann, N. E., Calle, L., Hurtt, G., Chatterjee, A., & Poulter, B.: Enhanced response of global wetland methane emissions to the 2015–2016 El Niño-Southern Oscillation event, Environ. Res. Lett., 13(7), 074009, https://doi.org/10.1088/1748-9326/aac939, 2018.

Zhao, Y., Saunois, M., Bousquet, P., Lin, X., Berchet, A., Hegglin, M. I., Canadell, J. G., et al.: Inter-model comparison of global hydroxyl radical (OH) distributions and their impact on atmospheric

methane over the 2000–2016 period, Atmos. Chem. Phys., 19(21), 13701–13723, https://doi.org/10.5194/acp-19-13701-2019, 2019.

Zhou, M., Langerock, B., Vigouroux, C., Sha, M. K., Ramonet, M., Delmotte, M., Mahieu, E., et al.: Atmospheric CO and CH_4 time series and seasonal variations on Reunion Island from ground-based in situ and FTIR (NDACC and TCCON) measurements, Atmos. Chem. Phys., 18(19), 13881–138901, https://doi.org/10.5194/acp-18-13881-2018, 2018.

Zhu, T., Melamed, M. L., Parrish, D., Gauss, M., Gallardo Klenner, L., Lawrence, M. G., Konare, A., & Liousse, C.: WMO/IGAC impacts of megacities on air pollution and climate, http://www.wmo.int/pages/prog/arep/gaw/documents/Final_GAW_205_web_31_January.pdf, 2012.